

Available online at www.sciencedirect.com**ScienceDirect**journal homepage: www.elsevier.com/locate/issn/15375110**Research Paper****Lighting systems and strategies compared in an optimally controlled greenhouse**

Wouter J.P. Kuijpers ^{a,*}, David Katzin ^b, Simon van Mourik ^b,
 Duarte J. Antunes ^a, Silke Hemming ^c, Marinus J.G. van de Molengraft ^a

^a Control Systems Technology Group, Eindhoven University of Technology, 5600 MB Eindhoven, Netherlands

^b Farm Technology Group, Wageningen University & Research, 6708 PB Wageningen, Netherlands

^c Greenhouse Horticulture, Wageningen University & Research, 6708 PB Wageningen, Netherlands

ARTICLE INFO**Article history:**

Received 29 June 2020

Received in revised form

27 November 2020

Accepted 10 December 2020

Published online 14 January 2021

Keywords:

Greenhouse environmental control

Carbon footprint

Artificial lighting

LED

Optimal control

LED lighting is appointed as the successor of HPS lighting in greenhouses since it can lead to a more sustainable cultivation, i.e. it converts electrical energy into photosynthetically active radiation more efficiently. To quantify the effect of this more efficient conversion within the operation of the greenhouse system, an optimal controller is proposed to generate optimal control trajectories for the controllable inputs of the greenhouse. The optimal controller makes use of an economic objective function, i.e. the difference between income ($yield \times product\ price$) and cost of resources ($resource\ use \times cost$). The performance of this optimally controlled greenhouse system is compared with respect to the state-of-the-practice. Simulation experiments suggest optimal control can increase the economic objective by 10 % to $65.14\ \text{€}\cdot\text{m}^{-2}$ compared to $58.96\ \text{€}\cdot\text{m}^{-2}$ for the state-of-the-practice, for tomatoes cultivated in a Dutch weather conditions. The model of the optimally controlled greenhouse is used to compare the performance of different lighting systems, i.e. no lighting, HPS lighting and LED lighting. An increase of 9 % in the operational return is observed for LED lighting compared to HPS lighting. The electricity that is saved due to the more energy-efficient conversion in the LED lighting results in a 30 % decrease in carbon footprint when comparing a greenhouse with LED lighting to a greenhouse with HPS lighting.

© 2020 The Author(s). Published by Elsevier Ltd on behalf of IAgE. This is an open access article under the CC BY license (<http://creativecommons.org/licenses/by/4.0/>).

1. Introduction

The cultivation of fruit and vegetables in greenhouses in the Netherlands consumes a vast amount of energy. From the total energy of 100.5 PJ consumed in 2018, 77 % was due to heating and 23 % due to electricity for artificial lighting (van der Velden & Smit, 2019). The Dutch horticultural industry

signed an agreement with the Dutch government to decrease the total energy consumption and its environmental footprint (van der Velden & Smit, 2019). One of the potential solutions for decreasing the environmental footprint of the horticultural industry is to reduce the electricity consumption by switching from High-Pressure Sodium (HPS) lighting to Light Emitting Diode (LED) lighting (Gómez & Mitchell, 2014).

* Corresponding author.

E-mail addresses: w.j.p.kuijpers@tue.nl (W.J.P. Kuijpers), david.katzin@wur.nl (D. Katzin), simon.vanmourik@wur.nl (S. van Mourik), d.antunes@tue.nl (D.J. Antunes), silke.hemming@wur.nl (S. Hemming), m.j.g.v.d.molengraft@tue.nl (M.J.G. van de Molengraft).

<https://doi.org/10.1016/j.biosystemseng.2020.12.006>

1537-5110/© 2020 The Author(s). Published by Elsevier Ltd on behalf of IAgE. This is an open access article under the CC BY license (<http://creativecommons.org/licenses/by/4.0/>).

Nomenclature	
<i>Sub- and Superscripts</i>	
\cdot_d	discretised signal or function
\cdot^*	optimal signal or value
\cdot^D	daily sum of signal
<i>Greek Symbols</i>	
α	thermal insulation constant of the heat buffer, s^{-1}
α_g	energy content per cube of gas, $J.m^{-3}$
α_{scr}	heat conductance of the screen, $J.m^{-1}.s^{-1}.^{\circ}C^{-1}$
α_{cov}	heat conductance of the cover, $J.m^{-1}.s^{-1}.^{\circ}C^{-1}$
γ_{boi}	contribution of boiler use to the carbon footprint, $kg.m^{-3}$
γ_{cby}	contribution of CO_2 bought to the carbon footprint, $kg.kg^{-1}$
γ_{eby}	contribution of electricity bought from grid to the carbon footprint, $kg.kWh^{-1}$
γ_{ese}	contribution of electricity sold to grid to the carbon footprint, $kg.kWh^{-1}$
Δ	quantisation factor, (–)
γ_{chp}	contribution of CHP use to the carbon footprint, $kg.m^{-3}$
η_{Ec}	fraction of CHP input power converted to electrical power, (–)
η_{Xb}	conversion of boiler input power to CO_2 output, gJ^{-1}
η_{Xc}	conversion of CHP input power to CO_2 output, gJ^{-1}
η_{X_Y}	fraction of input power to light source X converted to Y radiation, where $X \in \{led, hps, sun\}$ and $Y \in \{PAR, NIR\}$, (–)
θ_l	lower bound to inequality equations $h(\cdot)$
θ_u	upper bound to inequality equations $h(\cdot)$
Σ_x	reference to model component x
τ_l	discretization interval of the greenhouse system, s
τ_s	sampling interval of signals, s
$\phi_{c,ass}$	assimilation rate, $g.m^{-2}.s^{-1}$
<i>Alphabetical Symbols</i>	
a_{X_Y}	crop absorption for Y radiation from light source X, where $X \in \{led, hps, sun\}$ and $Y \in \{PAR, NIR\}$, (–)
A_{cov}	area of the greenhouse cover, m^2
A_{floor}	floor area of the greenhouse, m^2
c	vector of input unit prices
c_{boi}	cost of boiler gas, $\epsilon.m^{-3}$
c_{cby}	cost of pure CO_2 , $\epsilon.kg^{-1}$
c_{chp}	cost of CHP gas, $\epsilon.m^{-3}$
c_{eby}	cost of electricity from grid, $\epsilon.kWh^{-1}$
c_{ese}	return on sold electricity to grid, $\epsilon.kWh^{-1}$
c_{frt}	return on fruit harvest, $\epsilon.kg^{-1}$
c_w	heat capacity of water, $J.kg^{-1}.K^{-1}$
C_{buf}	crop carbohydrates in assimilate buffer, $g.m^{-2}$
C_{frt}	crop carbohydrates in fruit, $g.m^{-2}$
$C_{frt,off}$	offset in fruit buffer, $g.m^{-2}$
C_{leaf}	crop carbohydrates in leaves, $g.m^{-2}$
$CO_{2,air}$	greenhouse air CO_2 concentration, $g.m^{-3}$
$CO_{2,out}$	outside air CO_2 concentration, $g.m^{-3}$
d	uncontrollable inputs to the greenhouse system
d_A	thickness of the heat buffer wall, m
$f(\cdot)$	continuous time model of the greenhouse system
$f_{vmin}(\cdot)$	function describing the minimum ventilation rate as a function of wind speed, $m^3.m^{-2}.s^{-1}$
$f_{vmax}(\cdot)$	function describing the maximum ventilation rate as a function of wind speed, $m^3.m^{-2}.s^{-1}$
$F(\cdot)$	discrete time model of the greenhouse system, with sampling time τ_s
$\bar{F}(\cdot)$	discrete time model of the greenhouse system, with sampling time τ_l
g_c	condensation conductance of the cover, $m.s^{-1}$
$h(\cdot)$	inequality equations
H_a	energy loss from the heat buffer, $J.m^{-2}.s^{-1}$
H_{air}	greenhouse air humidity, $g.m^{-3}$
H_s	energy supplied to a released from the heat buffer, $J.m^{-2}.s^{-1}$
H_{out}	outside absolute air humidity, element in d, $g.m^{-3}$
i	integer variable
j	integer variable
J	optimised operational return, $\epsilon.m^{-2}$
k	extinction coefficient of the canopy, (–)
k_A	thermal conductivity of the heat buffer surface, $J.m^{-1}.s^{-1}.K^{-1}$
$l(\cdot)$	operational return of the greenhouse system, $\epsilon.m^{-2}$
LAI	leaf area index, $m^2.m^{-2}$
LAI_{max}	maximal leaf area index, $m^2.m^{-2}$
m_w	water mass, kg
$MC_{BuffFrt}$	assimilates partitioned to the fruit buffer, $g.m^{-2}.s^{-1}$
$MC_{LeafHar}$	leaf harvest, $g.m^{-2}.s^{-1}$
n_d	number of uncontrollable inputs
n_e	number of inequality constraints
n_u	number of inputs
n_x	number of states
N	prediction horizon
N_{sub}	number of subsamples
$p_1(\cdot)$	income through yield minus costs for gas, $\epsilon.m^{-2}$
$p_2(\cdot)$	carbon footprint, $kg.m^{-2}$
p_{g_c}	properties of the cover, $m.^{\circ}C^{-\frac{1}{2}}.s^{-1}$
$P(x)$	polynomial function in x
q	integer variable
Q_{cov}	convective heat loss through the cover, $J.m^{-2}.s^{-1}$
Q_{sun}	global radiation, element in d, $W.m^{-2}$
R_{PAR}	total PAR absorbed by the canopy, $W.m^{-2}$
R_{tot}	total radiation, PAR and NIR, absorbed by the canopy, $W.m^{-2}$
R_{X_Y}	Y radiation by lighting source X, where $X \in \{led, hps\}$ and $Y \in \{PAR, NIR\}$, $W.m^{-2}$
$s(\cdot)$	gas use function, $m^3.m^{-2}$
s_{boi}	gas use by boiler, $m^3.m^{-2}$
s_{chp}	gas use by CHP, $m^3.m^{-2}$
s_k^l	slope parameter in S, (–)
s_s	switching value parameter in S, (–)
s_v	value that determines value of S, (–)
$S(\cdot)$	smoothed if-else function by Vanthoor (2011)
SLA	specific leaf area, $g.m^{-2}$
t	time
t_0	start time of the optimal control horizon

t_f	end time of the optimal control horizon	u_{ven}	ventilation rate, $m^3 \cdot m^{-2} \cdot s^{-1}$
T_{air}	greenhouse air temperature, $^{\circ}\text{C}$	\mathbb{U}	set of admissible values for the inputs
T_{cov}	cover temperature, $^{\circ}\text{C}$	u_{wind}	outside wind speed, element in d , $m \cdot s^{-1}$
T_{c24}	24-hr average greenhouse air temperature, $^{\circ}\text{C}$	x	state vector of the greenhouse system
T_{out}	outside temperature, element in d , $^{\circ}\text{C}$	x_s	heat stored in heat buffer, $J \cdot m^{-2}$
u	controllable inputs to the greenhouse system	$x_{s,off}$	lowest energy content of the heat buffer, $J \cdot m^{-2}$
u_{boi}	the level of operation of the boiler, $W \cdot m^{-2}$	x_t	initial state
u_{cby}	(pure) CO_2 bought, $g \cdot m^{-2} \cdot s^{-1}$	\mathbb{X}	set of admissible values for the states
u_{chp}	the level of operation of the combined heat and power (CHP), $W \cdot m^{-2}$	y_c	effect of the crop on the greenhouse climate
u_{CO2}	greenhouse CO_2 injection, $g \cdot m^{-2} \cdot s^{-1}$	y_g	effect of the greenhouse climate on the crop
u_{eby}	electrical power bought, $W \cdot m^{-2}$		
u_{ese}	electrical power sold, $W \cdot m^{-2}$		
u_{frt}	fruit harvest, $g \cdot m^{-2} \cdot s^{-1}$		
u_g	controlled inputs to the greenhouse climate model		
u_{hea}	heating input to greenhouse, $J \cdot m^{-2} \cdot s^{-1}$		
u_{hps}	electrical power to HPS lighting, $W \cdot m^{-2}$		
u_{lea}	leaf harvest, $g \cdot m^{-2} \cdot s^{-1}$		
u_{led}	electrical power to LED lighting, $W \cdot m^{-2}$		
u_{scr}	screen set (1 represents fully deployed), (–)		
u_{sto}	energy flux to heat buffer, $W \cdot m^{-2}$		

simulation. The control strategy for the greenhouse aims at optimising the operational return defined as the difference between income ($\text{yield} \times \text{product prices}$) and cost of resources ($\text{resource use} \times \text{costs}$). Taking these steps, the two lighting systems can be compared.

Models have been developed for individual components of the greenhouse system, such as energy management system models (de Zwart, 1996; Seginer et al., 2018; van Beveren et al., 2019; van Ooteghem, 2007), greenhouse climate models (de Zwart, 1996; Katzin et al., 2020; van Beveren et al., 2015; Vanthoor, 2011) and crop growth and transpiration models (Heuvelink & Challa, 1989; Kuijpers et al., 2019; Vanthoor, 2011). The present paper builds upon the existing validated models, by combining them into a complete model for the greenhouse system. A set of existing models has been selected based on inclusion of physical and crop physiological phenomena and accuracy of validation. The complete greenhouse system model is validated with respect to the state-of-the-art, represented by economic figures in a reference budget (Vermeulen, 2016, p. 330), using a rule-based controller.

Several approaches to the greenhouse control challenge have been presented such as Hamiltonian maximization (Seginer et al., 2018), receding horizon optimal control (RHOC) (Ramírez-Arias et al., 2012; Tap, 2000; van Ooteghem, 2007) and optimal control using grower defined bounds (van Beveren et al., 2015). The present paper employs optimal control to provide a control strategy aimed at maximizing the operational return. The few published approaches that have employed an economic objective function use penalty factors, i.e. empirically determined factors converting undesirable configurations of the system (e.g. extreme temperatures) into an economic quantity. The economic quantity is used to penalise the occurrence of undesirable configurations through the objective function of the optimisation problem. In the approach proposed here, explainable white-box models are

Existing literature on HPS lighting and LED lighting mainly focusses at the energy conversion efficiency. For example, these lighting systems are compared in Nelson and Bugbee (2015) based on energy conversion efficiencies and in Dueck et al. (2012) and Gómez and Mitchell (2014) the lighting systems are compared in a greenhouse experiment with tomatoes. Data from the experiment by Dueck et al. (2012) has been used to evaluate a model by Katzin et al. (2020) which aims to describe the qualitative difference between HPS lighting and LED lighting. Xu, Wei, & Xu, 2019 proposed a switching strategy for turning on and off LED lights using multi-objective optimisation is proposed, reporting an energy reduction of 30% with respect to rule-based control. Other research into the effects on crop growth by Lee et al. (2014) and Olle and Virsile (2013) and optimal positioning of the lighting system by Ferentinos and Albright (2005), solely focuses on LED lighting, not on HPS lighting. Overall, LED lighting is attributed a higher efficiency in converting electrical power to photosynthetically active radiation (PAR). The installed electrical capacity of LED lighting can be lower while achieving similar levels of PAR, while emitting less radiative energy.

This paper provides insight on to what extent LED lighting improves the performance of an optimally controlled greenhouse system, measured in operational return ($\text{yield income} - \text{resource costs}$) and carbon footprint. To this extent, this paper will quantify the difference in operational return and carbon footprint in simulations using an optimally controlled greenhouse with HPS and LED lighting. The control inputs to the greenhouse result from an optimisation problem which ensures a fair comparison between both lighting systems. Towards this end, a model is developed that predicts the effect of the lighting systems on the crop, the greenhouse climate and the production of electricity for the lighting systems. As a lighting system influences the greenhouse climate, all relevant inputs e.g. heating, must also be included in this

used to estimate the effect of an undesirable configuration of the system. In Xu et al. (2018) also an economic objective function without penalty factors is considered. However, with respect to the aim of this paper a model detailing the origin of electricity and heat is not present in Xu et al. (2018) which therefore follows a different approach.

The contribution of this paper is four-fold. A model, capable of describing how the inputs to the greenhouse system (including the energy management system and artificial lighting) affect the crop growth and production, is selected and the interconnection is validated using data representing the state-of-the-practice. Secondly, an optimal control algorithm is proposed which, in combination with the aforementioned model, can control the greenhouse system using a purely economic cost function (no penalty functions). Thirdly, the effects of different lighting systems employed in the greenhouse system are analysed, and conclusions are drawn with respect to the potential economic benefits and carbon footprint reduction of LED lighting in tomato greenhouses. Lastly, the effect of the quantisation in the system, due to the ability of only switching on/off the lighting is researched, aiming to increase the accuracy of the third contribution by removing the assumption that the lights can be controlled to attain any value.

The remainder of this paper is organised as follows, Section 2 will elaborate on the selected models, the interconnection of the selected models and the control of the greenhouse system. The simulation studies will be presented in Section 3 and the results will be discussed in Section 4. Directions for future work and the conclusion of this research are presented in Section 5.

2. Models & methods

In order to be able to compare various lighting systems, a model is developed to predict the effect of a lighting system on the operation of the greenhouse system. As a different lighting system might also affect the selected greenhouse climate control strategy, the controlled greenhouse system must be considered. The greenhouse control problem is presented in subsection 2.1. The model used to simulate the greenhouse system, consists of three parts, the energy management system, the greenhouse climate and lighting system and crop growth and transpiration, these are detailed in subsection 2.2, 2.3, 2.4 and 2.5, respectively. The derivation of the economic objective function is detailed in subsection 2.6. The implementation of the proposed controller is presented in subsection 2.7. The rule-based controller used in the validation of the model is presented in subsection 2.8. The relevant data from the state-of-the-practice and the weather data are presented in subsection 2.9 and 2.10, respectively.

2.1. Greenhouse control problem

The greenhouse control problem is graphically represented by the block diagram as depicted in Fig. 1. The model of the greenhouse system is composed of the energy management system Σ_E , greenhouse climate and lighting system model Σ_G and crop growth and transpiration model Σ_C . The greenhouse system is affected by controllable inputs $u \in \mathbb{R}^{n_u}$ and

uncontrollable inputs $d \in \mathbb{R}^{n_d}$. The interaction between the greenhouse climate model and the crop (temperature, CO₂ concentration, radiation and relative humidity) and vice versa (assimilation and transpiration), are denoted by y_g and y_c in Fig. 1, respectively. The controlled inputs to the greenhouse climate model are represented by u_g . The dynamical model of the system is represented by

$$\dot{x}(t) = f(x(t), u(t), d(t)), \quad (1)$$

where $x(t) \in \mathbb{R}^{n_x}$ is the state of the greenhouse system.

For the simulations presented in this paper, the inputs to the greenhouse system u will result from an optimisation problem run by controller Σ_M . The controller optimises the operational return $l(u(t), c(t)) : \mathbb{R}^{n_u} \times \mathbb{R}^{n_u} \rightarrow \mathbb{R}$ over a horizon $t \in [t_0, t_f]$, referred to as the prediction horizon. The prediction horizon has to be larger than the timescales of the relevant slow dynamics of the system F , to be able to properly optimise the control inputs. The cost/return of a unit input is $c(t) \in \mathbb{R}^{n_u}$, i.e. $c_i(t)u_i(t)$ represents the contribution of input $i \in \{1, \dots, n_u\}$ to the operational return and is expressed in monetary units. This is mathematically represented by

$$J(x_t) = \max_{u(t)} \int_{t_0}^{t_f} l(u(t), c(t)) dt \quad (2)$$

subject to :

$$\dot{x}(t) = f(x(t), u(t), d(t))$$

$$(x(t), u(t)) \in \mathbb{X} \times \mathbb{U},$$

$$\theta_l \leq h(x(t), u(t)) \leq \theta_u, \quad \text{for } t \in [t_0, t_f]$$

$$x(t_0) = x_t,$$

where $x_t \in \mathbb{R}^{n_x}$, represents the state at $t = t_0$. $x(t)$ is the state of the actual greenhouse system at time t . The controller is assumed to have full state information. The inequality equations are expressed in terms of functions $h(\cdot)$ which are lower and upper bounded by $\theta_l \in \mathbb{R}^{n_e}$ and $\theta_u \in \mathbb{R}^{n_e}$ respectively. The sets $\mathbb{X} \subset \mathbb{R}^{n_x}$ and $\mathbb{U} \subset \mathbb{R}^{n_u}$ represent admissible values for the states and inputs, respectively.

All bounds are fixed except for the bounds on the ventilation rate control input u_{ven} . The bounds on u_{ven} , $f_{umin}(\cdot) : \mathbb{R} \rightarrow \mathbb{R}$ and $f_{umax}(\cdot) : \mathbb{R} \rightarrow \mathbb{R}$, originate from the model in chapter 6 of de Jong (1990) and depend on the wind speed, a similar approach as presented in van Beveren et al. (2015). The states x and inputs u for the model in (1), are listed in Tables 1 and 2, respectively. The values of states and inputs will be presented per square meter of ground area. The upper bound of the carbohydrates buffer in the leaves C_{leaf} , is determined by maximal leaf area index input by the user LAI_{max} , in this paper $LAI_{max} = 3 \text{ m}^2 \cdot \text{m}^{-2}$ and $SLA = 26.6 \text{ kg} \cdot \text{m}^{-2}$ (Vanhoor, 2011). The lower bound of the fruit carbohydrates buffer C_{frt} is set to $C_{frt,off}$, see subsection 2.5.

Subsections 2.2, 2.3, 2.4 and 2.5 present the three components of the model in (1), depicted in Fig. 1. The subsections start with an introduction of the model that is used and afterwards elaborate on the changes made to these models. The changes to

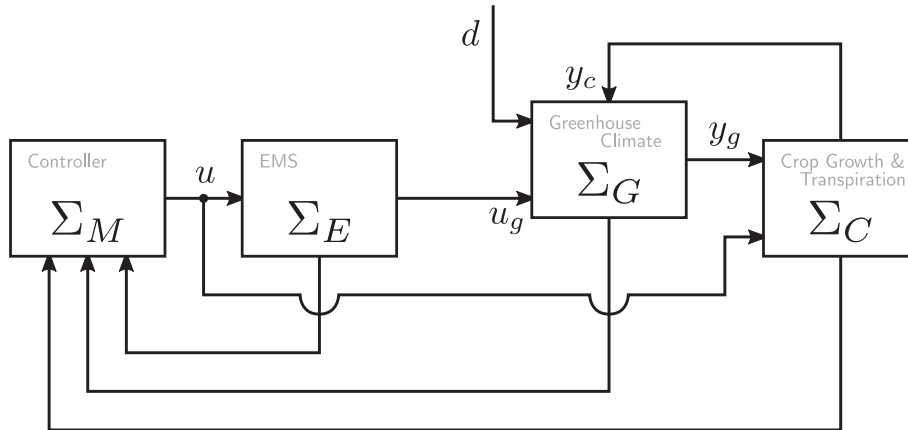


Fig. 1 – Block diagram representation of the greenhouse control problem, composed of controller Σ_M , energy management system Σ_E , greenhouse climate and lighting system model Σ_G and crop growth and transpiration model Σ_C . The control inputs to the greenhouse system are denoted by u , the elements input to Σ_C encompass the harvest of fruits and leaves. The controlled inputs to the greenhouse climate model are denoted by u_g , see (6). The uncontrolled inputs to the greenhouse climate model are denoted by d , the outside weather. Variables y_g and y_c denote the effect of the greenhouse climate on the crop (temperature, CO₂ concentration, radiation and relative humidity) and the effect of the crop on the greenhouse (assimilation and transpiration), respectively.

the models mostly encompass removing discontinuities from the models and ensuring continuous differentiability. Discontinuities and a deficient degree of continuous differentiability will generally decrease the performance of the gradient-based optimisation methods and were therefore avoided whenever possible. The parameters of the models have been taken in accordance with the publication in which the models have been validated (Seginer et al., 2018; van Beveren et al., 2015; Vanthoor, 2011) unless stated otherwise.

2.2. Energy management system

As a different lighting system might also affect the use of resources, the energy management system is a crucial component in the greenhouse system model. The model of the energy management system is based on the model presented in Seginer et al. (2018) and is composed of a combined heat and power unit (CHP), a boiler and a heat buffer. This model has one state x_s which represents the stored heat in the buffer. The buffer is supplied and depleted using control input u_{sto} . The inputs to this model encompass the setpoints given to the CHP (u_{chp}) and boiler (u_{boi}). Pure CO₂ is bought (u_{cby}) to compensate for a difference between the CO₂ produced on-

site (CHP and boiler) and the injection rate (u_{CO_2}). Electricity is bought (u_{eb}) and sold (u_{es}) to counterbalance the difference between the electricity demand by the lighting (u_{hps} and u_{led}) and electricity generated on-site (CHP).

The model itself only contains dynamics related to the heat buffer. The description for the energy loss from the heat buffer H_a (W·m⁻²) was changed from a discontinuous description to a continuously differentiable description

$$H_a = -\alpha \cdot x_s \quad (3)$$

where x_s (J·m⁻²) represents the energy stored in the buffer, see Table 1. The lowest energy content in the heat buffer is represented by a constant value $x_{s,off} \in \mathbb{R}$ (J·m⁻²). The thermal insulation constant is represented by α . With this proposed new description, H_a is now a function of x_s more accurately describing the energy loss when storing energy in the heat buffer for a long time, as indicated by Seginer et al. (2018). The derivation of the thermal insulation $\alpha = 3.96 \cdot 10^{-7}$ (s⁻¹) is presented in Appendix A.

The fraction of the input power to the CHP that is converted to electrical power is given by $\eta_{Ec} = 0.4$ (–) (Seginer et al., 2018), the balance of produced and consumed electricity is therefore

Table 1 – States in the greenhouse system model x and corresponding constraints represented by lower and upper bounds.

States $x = [x_s; T_{air}; H_{air}; CO_{2,air}; C_{buf}; C_{leaf}; C_{frt}; T_{c24}]$	Symbol	Lower bound	Upper bound	Unit	Description
x_s		0	$3 \cdot 10^6$	J·m ⁻²	heat stored in heat buffer
T_{air}		10	35	°C	greenhouse air temperature
H_{air}		5	35	g{H ₂ O}·m ⁻³	greenhouse air humidity
$CO_{2,air}$		0.69	2.79	g{CO ₂ }·m ⁻³	greenhouse air CO ₂ concentration
C_{buf}		0	20	g(CH ₂ O)·m ⁻²	crop carbohydrates in assimilate buffer
C_{leaf}		0	LAI_{max}/SLA	g(CH ₂ O)·m ⁻²	crop carbohydrates in leaves
C_{frt}		$C_{frt,off}$	∞	g(CH ₂ O)·m ⁻²	crop carbohydrates in fruit
T_{c24}		10	35	°C	24-hr average greenhouse air temperature

Table 2 – Inputs to the greenhouse system model u and corresponding constraints represented by lower and upper bounds.

Symbol	Lower bound	Upper bound	Unit	Description
u_{chp}	0	125	$W.m^{-2}$	the level of operation of the combined heat and power (CHP)
u_{boi}	0	83.33	$W.m^{-2}$	the level of operation of the boiler
u_{hps}	0	100	$W.m^{-2}$	electrical power to HPS lighting
u_{led}	0	61.67	$W.m^{-2}$	electrical power to LED lighting
u_{eby}	0	250	$W.m^{-2}$	electrical power bought
u_{ese}	0	250	$W.m^{-2}$	electrical power sold
u_{CO2}	0	250	$g\{CO_2\}.m^{-2}.s^{-1}$	greenhouse CO_2 injection
u_{cby}	0	250	$g\{CO_2\}.m^{-2}.s^{-1}$	(pure) CO_2 bought
u_{sto}	– 250	250	$W.m^{-2}$	energy flux to heat buffer
u_{ven}	$f_{vmin}(d)$	$f_{vmax}(d)$	$m^3.m^{-2}.s^{-1}$	ventilation rate
u_{scr}	0	1	–	screen set (1 represents fully deployed)
u_{lea}	0	$0.4 \cdot 10^{-6}$	$g\{CH_2O\}.m^{-2}.s^{-1}$	leaf harvest
u_{frt}	0	$0.4 \cdot 10^{-4}$	$g\{CH_2O\}.m^{-2}.s^{-1}$	fruit harvest

$$\eta_{Ec}u_{chp} + u_{eby} - u_{ese} - u_{hps} - u_{led} = 0, \quad (4)$$

and it is added to the constraints, $h(x(t), u(t))$ in (2), by setting $\theta_{i,i} = \theta_{u,i} = 0$ for the corresponding constraint i . Also, the balance equation for the CO_2 is added to the constraint equation

$$\eta_{Xc}u_{chp} + \eta_{Xb}u_{boi} + u_{cby} - u_{CO2} = 0, \quad (5)$$

here $\eta_{Xc} = 7.22 \cdot 10^{-5}$ (–) and $\eta_{Xb} = 7.22 \cdot 10^{-5}$ (–) (Seginer et al., 2018) represent the production of CO_2 per unit of energy that is consumed by the CHP and the boiler, respectively. A similar constraint has been added to match heat supply and demand. The output to the greenhouse climate model u_g (see Fig. 1).

$$u_g = [u_{hea}; u_{CO2}; u_{hps}; u_{led}; u_{scr}; u_{ven}], \quad (6)$$

where u_{hea} ($W.m^{-2}$) and u_{CO2} ($g.m^{-2}.s^{-1}$) refer to the resulting heat flux to the heating pipes and the CO_2 injection rate.

2.3. Lighting system

In the present paper, three different lighting systems are compared no lighting, HPS lighting and LED lighting. To allow for a comparison with respect to economic figures in budget G56 in KWIN (Vermeulen, 2016, p. 330), the photosynthetic photon flux density (PPFD) of HPS lighting used in this research matches that of budget G56, $185 \mu mol.s^{-1}.m^{-2}$. In KWIN, the HPS electrical input power is $100 W.m^{-2}$, resulting in an efficacy of $1.85 \mu mol.J^{-1}$. For the sake of comparison, the PPFD of LED lighting is modelled as $185 \mu mol.s^{-1}.m^{-2}$, with an efficacy of $3 \mu mol.J^{-1}$ (Kusuma et al., 2020). The models are part of the greenhouse climate and lighting system model Σ_G , in Fig. 1.

In this research, all electrical energy input to the lights is modelled to contribute to the energy balance. The energy used to transpire water in the crop, the latent heat, is accounted for in the transpiration model. The lamps are modelled to radiate both PAR and near-infrared (NIR), the radiation is described by

$$R_{XY} = \eta_{XY}u_X, \quad (7)$$

where $X \in \{led, hps\}$ and $Y \in \{PAR, NIR\}$. The fraction of the electrical input of the lights that is converted to PAR is represented by $\eta_{LEDPAR} = 0.55$ (–) and $\eta_{HPSPAR} = 0.35$ (–) according to Katzin et al. (2021). The fraction of the electrical input of the lights that is converted to NIR is chosen $\eta_{LEDNIR} = 0.02$ (–) and $\eta_{HPSNIR} = 0.22$ (–) according to Katzin et al. (2021).

The total PAR absorbed by the canopy R_{PAR} ($W.m^{-2}$) is given by,

$$R_{PAR} = (1 - e^{-k \cdot LAI}) (a_{sun_{PAR}} \eta_{sun_{PAR}} Q_{sun} + a_{LED_{PAR}} R_{LED_{PAR}} + a_{HPS_{PAR}} R_{HPS_{PAR}}), \quad (8)$$

where k (–) is the extinction coefficient of the canopy for PAR, LAI ($m^2.m^{-2}$) the leaf area index and Q_{sun} ($W.m^{-2}$) the global radiation in d . The total PAR absorbed by the canopy R_{PAR} is substituted for PAR_{Can} in the photosynthesis model in equation (9.14) of Vanthoor (2011), which is part of the crop growth model presented in subsection 2.5. The fraction of PAR in the global radiation $\eta_{sun_{PAR}} = 0.44$ (–), according to Nelson and Bugbee (2015). The absorption parameters have been chosen $a_{sun_{PAR}} = 0.894$ (–), $a_{LED_{PAR}} = 0.943$ (–) and $a_{HPS_{PAR}} = 0.870$ (–) according to Nelson and Bugbee (2015).

The total radiation R_{tot} ($W.m^{-2}$), PAR and NIR, absorbed by the crop is described by

$$R_{tot} = R_{PAR} + (1 - e^{-k \cdot LAI}) (a_{sun_{NIR}} \eta_{sun_{NIR}} Q_{sun} + a_{LED_{NIR}} R_{LED_{NIR}} + a_{HPS_{NIR}} R_{HPS_{NIR}}), \quad (9)$$

where R_{tot} is substituted for R_n in Equations (8) and (10) of van Beveren et al. (2015), which is part of the greenhouse climate system model presented in subsection 2.4. The fraction of NIR in the global radiation is set to $\eta_{sun_{NIR}} = 0.5$ (–), according to Vanthoor (2011). The absorption parameters have been chosen $a_{sun_{NIR}} = 0.214$ (–), $a_{LED_{NIR}} = 0.923$ (–) and $a_{HPS_{NIR}} = 0.263$ (–) according to Nelson and Bugbee (2015).

In the simulation studies with this model, three lighting systems are compared. For simulations with no lighting, u_{led} and u_{hps} are zero. For simulations with HPS, u_{led} is zero and for

simulations with LED lighting u_{hps} is zero. To make a realistic comparison, the PAR output of both types is chosen equal, $185 \mu\text{mol.s}^{-1}.\text{m}^{-2}$, but different input power ratings u_{hps} and u_{led} are employed, $100 \text{J.m}^{-2}.\text{s}^{-1}$ and $61.67 \text{J.m}^{-2}.\text{s}^{-1}$, respectively, see Table 2.

The typical electrical implementation of the artificial lighting systems in practice only allows for switching lamps on or off, no value in-between. The control inputs u_{hps} and u_{led} resulting from (2) have a continuous domain, i.e. they can take any value between the bounds in Table 2. This restriction can be modelled by a quantisation process, applied to the control input. A viable method to obtain a value in between is to only switch on a spatially distributed group of lights, e.g. one third of the total amount of lights, in which way the average radiation per square meter will be one third of the bounds in Table 2. In the simulation study presented here, the effect of this quantisation on the performance of the controlled system will be analysed for a system with no quantisation, a system with two possible values, referred to as $\Delta = 1$ and a system with four possible values, referred to as $\Delta = 1/3$.

2.4. Greenhouse climate system

The greenhouse climate system creates a favourable climate, represented by y_g in Fig. 1, for crop growth. The model predicts the greenhouse climate based on the control inputs u_g , defined in (6). The model of the greenhouse climate is based on the model presented in van Beveren et al. (2015). The model consists of an energy balance, absolute humidity balance and CO_2 balance. The absolute humidity balance is affected by crop transpiration and the CO_2 balance by crop assimilation, both quantities are contained in y_c , see Fig. 1. The outside radiation Q_{sun} (W.m^{-2}), temperature T_{out} ($^{\circ}\text{C}$), absolute humidity H_{out} (g.m^{-3}), CO_2 concentration $\text{CO}_{2,\text{out}}$ (g.m^{-3}), and wind speed v_{wind} (m.s^{-1}) are contained in d , affect the various balances.

The model for condensation conductance g_c (m.s^{-1}) of the cover, the temperature of which is denoted by T_{cov} ($^{\circ}\text{C}$), is based on the model by Stanghellini and de Jong (1995) given by,

$$g_c = \max\left(0, p_{g_c} (T_{\text{air}} - T_{\text{cov}})^{\frac{1}{3}}\right), \quad (10)$$

by van Beveren et al. (2015) is not continuously differentiable due to the \max operator. Parameter p_{g_c} represents the specific properties of the cover ($\text{m.}^{\circ}\text{C}^{-\frac{1}{3}}.\text{s}^{-1}$). To ensure the continuous differentiability of (10), the \max operator is replaced by the approximation of a smoothed if-else function $S : \mathbb{R}^3 \rightarrow \mathbb{R}$, proposed by Vanthoor (2011).

$$S(s_v, s_k^l, s_s) = \frac{1}{1 + e^{s_k^l(s - s_s)}}, \quad (11)$$

where s_k^l (–) and s_s (–) represent the slope and the switching value of the smoothed if-else. In (11), s_v (–) represents the value that determines the value of S . To smooth (10), we choose $s_v = (T_{\text{air}} - T_{\text{cov}})$, $s_s = 1^{\circ}\text{C}$ and $s_k^l = -2$. The third-order

root is approximated by a fourth-order polynomial, represented here by $P : \mathbb{R} \rightarrow \mathbb{R}$, defined as

$$P(x) = -4.03 \cdot 10^{-5} \cdot x^4 + 2.4 \cdot 10^{-3} \cdot x^3 - 0.05 \cdot x^2 + 0.49 \cdot x + 0.30. \quad (12)$$

Resulting in

$$g_c = p_{g_c} \cdot S((T_{\text{air}} - T_{\text{cov}}), -2, 1) \cdot P(T_{\text{air}} - T_{\text{cov}}). \quad (13)$$

The error introduced due to the approximation of g_c in (13) is at most 0.7 m.s^{-1} in the interval $-\infty < (T_{\text{air}} - T_{\text{cov}}) < 28^{\circ}\text{C}$. The model of the convective heat loss through the cover, Q_{cov} ($\text{J.m}^{-2}.\text{s}^{-1}$) in van Beveren et al. (2015), is extended with an energy screen. The screen and the greenhouse cover are modelled as two heat conductors in a series composition

$$Q_{\text{cov}} = \frac{1}{(u_{\text{scr}} \alpha_{\text{scr}})^{-1} + \left(\alpha_{\text{cov}} \frac{A_{\text{cov}}}{A_{\text{floor}}}\right)^{-1}} (T_{\text{air}} - T_{\text{out}}), \quad (14)$$

where the term $\alpha_{\text{cov}} \frac{A_{\text{cov}}}{A_{\text{floor}}}$ denotes the conductance of the greenhouse cover, in which A_{cov} and A_{floor} denote the greenhouse cover and floor area, respectively, with $A_{\text{cov}} \cdot (A_{\text{floor}})^{-1} = 1.29$. The value of the heat conductance of the screen $\alpha_{\text{scr}} = 9.33 (\text{W.m}^{-1} \text{C}^{-1})$ and has been taken in accordance with Seginer et al. (2018), the value of the heat conductance of the greenhouse cover $\alpha_{\text{cov}} = 5.00 (\text{W.m}^{-1} \text{C}^{-1})$ in accordance with van Beveren et al. (2015). Lastly, the models for assimilation, $\varphi_{\text{c,ass}}$ ($\text{g.m}^2.\text{s}^{-1}$) in van Beveren et al. (2015), are replaced by the models for assimilation by Vanthoor (2011), for the sake of coherence with respect to the chosen crop growth model.

To ensure the greenhouse air relative humidity is bounded between 10% and 95%, an additional constraint is added, in $h(x(t), u(t))$ in (2). The heat and radiation generated by the lighting is modelled to affect the greenhouse energy balance according to subsection 2.3. The output of the greenhouse climate model to the crop model, y_g in Fig. 1, is a vector containing

$$y_g = [R_{\text{PAR}}; R_{\text{tot}}; T_{\text{air}}; H_{\text{air}}; \text{CO}_{2,\text{air}}] \quad (15)$$

where R_{PAR} and R_{tot} are as defined in (8) and (9). T_{air} , H_{air} and $\text{CO}_{2,\text{air}}$ belong to the states of this model, see Table 1.

2.5. Crop growth and transpiration

The crop model predicts the growth, transpiration and respiration of the crop based on the greenhouse climate, y_g in (15). The crop model employed in this paper is based on the model by Vanthoor (2011). The model by Vanthoor predicts the assimilate content of the assimilate buffer (C_{buf}), the leafs (C_{leaf}), the stem and roots and the fruits (C_{frt}), the states of the model. The prediction of transpiration and assimilation of the crop, represented by y_c in Fig. 1, are output to the greenhouse climate system. The model describes how PAR R_{PAR} , greenhouse air temperature T_{air} and greenhouse air CO_2 concentration $\text{CO}_{2,\text{air}}$ affect the crop growth, also the effect of undesirable temperatures is

included in the model by [Vanhoor \(2011\)](#) through growth inhibition functions.

The model by Vanhoor employs a fixed boxcar train method to model the development of the fruit between fruit set and harvest. The expected increase in accuracy by using this method compared to directly selling the partitioned assimilates does not outweigh the additional (near-)discontinuities and extra state variables. To model the amount of fruits produced, the description of the assimilates partitioned to the fruits $MC_{Buf_{frt}} (g.m^{-2}.s^{-1})$ by Vanhoor is used. The controller will then optimise the climate for fruit growth (assimilates partitioned to the fruit buffer C_{frt}). Fruit development will, however, be guaranteed as the climate for fruit development does not differ significantly from the climate for fruit set. To cope with the development time for fruit a strategy similar to [Seginer et al. \(2018\)](#) is employed: all assimilates partitioned to the fruits minus those used for maintenance respiration, are counted as yield. The price for which it is sold at the time instance of partitioning is the price 30 days after this time instance. This is in line with the observation in chapter 3 of [Heuvelink \(2018\)](#), where a harvested fruit has already had the majority of its assimilates transported 30 days after fruit set. The part of the model by Vanhoor that describes the assimilate content of the stem and roots is removed as it does not affect the objective function.

The model by Vanhoor also describes leaf harvest using a (smoothed) if-else model to compare the current leaf area index to a maximal leaf area index. To avoid the (smoothed) discontinuity and allow for more freedom for the controller, the $MC_{LeafHar} (g.m^{-2}.s^{-1})$ in Vanhoor is replaced by a control input u_{lea} . To impose a maximal leaf area index LAI_{max} , a state constraint on C_{leaf} was added, see [Table 1](#). Also, the fruit harvest is selected as a control input u_{frt} . A state constraint is imposed $C_{frt} > C_{frt,off}$. The offset $C_{frt,off} = 140 g.m^{-2}$, represents the estimated fixed amount of developing fruit biomass on the crop and results in a more realistic fruit maintenance respiration compared to $C_{frt,off} = 0 g.m^{-2}$.

The transpiration model of Vanhoor requires the vapour pressure of the canopy which is not modelled by the greenhouse climate model presented in the subsection 2.4. The transpiration model used in this research is the one by [van Beveren et al. \(2015\)](#).

2.6. Performance models

The controller (Σ_M in [Fig. 1](#)) aims to optimise the operational return by proposing a control strategy for the inputs of the greenhouse system, u in [Fig. 1](#). Here, the operational return is defined as

$$l(u, c) = c_{frt} \cdot u_{frt} + c_{ese} \cdot u_{ese} - c_{chp} \cdot u_{chp} - c_{boi} \cdot u_{boi} - c_{cby} \cdot u_{cby} - c_{eby} \cdot u_{eby}, \quad (16)$$

where c_{xxx} represents the unit cost of input u_{xxx} . The (positive) inputs u_{chp} , u_{boi} , u_{eby} and u_{cby} , represent the resource use and these therefore lead to a decrease in the objective function $l(\cdot)$. Selling electrical power u_{ese} and fruit yield u_{frt} lead to an increase of the objective function. The operational return only reflects the costs and incomes relevant through the inputs

specified in [Table 2](#), fixed or capital costs are not included. Thus, e.g. the capital cost difference between a LED installation as compared to an HPS installation are not included.

To allow for comparison with respect to economic figures in budget G56 in KWIN ([Vermeulen, 2016](#), p. 330), the parameterisation of the objective function, c_{chp} , c_{boi} , c_{cby} , c_{ese} , c_{eby} and c_{frt} in [\(16\)](#), is taken according to the values in KWIN. Values for parameters taken from KWIN are given in subsection 2.9 ([Table 3](#)). The electricity bought (u_{eby}), electricity sold (u_{ese}) and the CO₂ bought (u_{cby}) in KWIN are not specified on a 4-weekly period basis, for these values only a seasonal total is presented. When comparing operational return to the KWIN, we assume that the average value of the evaluated period is equal to the seasonal average. To allow for a more detailed comparison of the yield versus gas use trade-off, the values available in KWIN on a 4-weekly basis are combined into the p_1 -performance $p_1(\cdot) : \mathbb{R}^{n_u} \times \mathbb{R}^{n_u} \rightarrow \mathbb{R}$

$$p_1(u, c) = c_{frt} \cdot u_{frt} - c_{chp} \cdot u_{chp} - c_{boi} \cdot u_{boi}. \quad (17)$$

The p_1 -performance represents income through yield minus cost of gas use and consists of a subset of terms in the operational return in [\(16\)](#).

Apart from the performance indicators $l(\cdot)$ and $p_1(\cdot)$, simulations will also be compared based on gas use $s(\cdot) : \mathbb{R}^{n_u} \rightarrow \mathbb{R}$

$$s(u) = \alpha_g^{-1} (u_{chp} + u_{boi}), \quad (18)$$

where $\alpha_g = 31.65 \text{ MJ.m}^{-3}$ ([Vermeulen, 2016](#), p. 330) represents the energy content per cube of gas. The gas use is defined here as a separate performance indicator, but is also required for both $l(\cdot)$ and $p_1(\cdot)$ and is included in c_{chp} and c_{boi} .

Additionally, simulations are compared based on environmental footprint $p_2(\cdot) : \mathbb{R}^{n_u} \times \mathbb{R}^{n_u} \rightarrow \mathbb{R}$ expressed in kilograms of CO₂ equivalents per square meter greenhouse area (kg.m^{-2}),

$$p_2(u, \gamma) = \gamma_{boi} \cdot s_{boi} + \gamma_{chp} \cdot s_{chp} + \gamma_{cby} \cdot u_{cby} + \gamma_{eby} \cdot u_{eby} - \gamma_{ese} \cdot u_{ese}. \quad (19)$$

The contribution of a unit input to the carbon footprint p_2 is $\gamma \in \mathbb{R}^{n_u}$, i.e. $\gamma_i u_i(t)$ represents the contribution of input $i \in \{1, \dots, n_u\}$ to the carbon footprint and is expressed in kilograms of CO₂ equivalents. The gas use by the boiler is denoted by $s_{boi} \in \mathbb{R} (m^3.m^{-2})$, gas use by the CHP by $s_{chp} \in \mathbb{R} (m^3.m^{-2})$. The gas use by the boiler s_{boi} is calculated using [\(18\)](#) for $u_{chp} = 0$, and vice versa for the gas use by the CHP s_{chp} . Also, for comparisons between simulations and the KWIN based on environment footprint p_2 assumed is that the average value of the evaluated period is equal to the seasonal average, due to unavailability of more detailed data.

2.7. Control approach

This subsection describes the approach for implementing optimal control according to the optimisation problem in [\(2\)](#). The inputs to the greenhouse system u can typically be updated every 15 min, $\tau_l = 15 \cdot 60 = 900 \text{ s}$, and are held constant in-between samples. For the sake of computational efficiency, the greenhouse model and the objective function are discretised using a zero-order hold with discretization interval

Table 3 – The weights used to multiply the control inputs with to arrive at the performance indicators operational return, weights c_{chp} , c_{boi} , c_{cby} , c_{ese} , c_{eby} and c_{frt} , and environmental footprint, weights γ_{boi} , γ_{chp} , γ_{cby} , γ_{ese} and γ_{eby} . Crop price c_{frt} varies throughout the season between 0.74 in summer and 1.92 euro.kg⁻¹ in winter. These values originate from the KWIN (Vermeulen, 2016, p. 330).

Operational Return [euro.m ⁻²]					
c_{frt}	[0.74 – 1.92]	euro.kg ⁻¹	c_{boi}	0.19	euro.m ⁻³
c_{ese}	0.037	euro.kWh ⁻¹	c_{eby}	0.057	euro.kWh ⁻¹
c_{chp}	0.17	euro.m ⁻³	c_{cby}	0.11	euro.kg ⁻¹
Environmental Footprint [kg.m ⁻²]					
γ_{boi}	1.87	kg.m ⁻³	γ_{eby}	0.64	kg.kWh ⁻¹
γ_{chp}	2.25	kg.m ⁻³	γ_{ese}	0.57	kg.kWh ⁻¹
γ_{cby}	1	kg.kg ⁻¹			

τ_l . As the employed solver in this research works efficiently with sparse problems (Wächter & Biegler, 2006), the optimisation problem is presented to the solver in a multiple-shooting formulation. Reformulation of the optimal control problem in (2) according to the latter steps, yields

$$J(x_t) = \max_{u_d(\cdot|i)} \sum_{j=0}^N l_d(u_d(j|i), c(j|i)), \quad (20)$$

subject to:

$$x_d(j+1|i) = F(x_d(j|i), u_d(j|i), d(j|i)),$$

$$(x_d(j|i), u_d(j|i)) \in \mathbb{X} \times \mathbb{U},$$

$$\theta_l \leq h(x_d(j|i), u_d(j|i)) \leq \theta_u, \quad \forall j = \{0, \dots, N\}$$

$$x_d(0|i) = x_t,$$

where $u_d(j|i) := u(j\tau_l|i\tau_l)$ is the predicted $(k|t) \cdot (k+t)$ sampled input signal u at future discrete steps $(j+i)\tau_l$ computed at time $i\tau_l$. Similarly, $x_d(j|i) := x(j\tau_l|i\tau_l)$ and $d_d(j|i) := d(j\tau_l|i\tau_l)$ represent the predicted sampled state x and predicted disturbance d . The discretised system, $F(\cdot)$, is obtained by a zero-order hold discretization of the system in (1) with discretization interval τ_s (s).

As the state of the system x_d will evolve as predicted by propagation of F , i.e. there is no uncertainty or model mismatch, an update step of 1 day is considered sufficient. The algorithm in (20) is thus recomputed every day using the state at that moment x_t , after which the first day of the optimised trajectories in u_d is applied to the system.

To ensure all (fast) physical phenomena are accurately represented by the discretised system by the map $F(\cdot)$ which runs at a smaller sampling period, $\tau_s < \tau_l$ with $\tau_s = \tau_l \cdot N_{sub}^{-1}$, where $N_{sub} \geq 1$ and N_{sub} is assumed to take on integer values. By this we mean that, given the control inputs $u_d(j|i)$ and $d_d(j|i)$, $F(\cdot)$ maps $x_d(j|i)$ into $x_d(j+1|i)$ according to

$$x_d((q+1)\tau_s + (j+i)\tau_l | i\tau_l) = \bar{F}(x_d(q\tau_s + (j+i)\tau_l | i\tau_l), u_d(j|i)d_d(j|i)), \quad q \in \{0, \dots, N_{sub} - 1\}, \quad (21)$$

with

$$x_d((j+i)\tau_l | i\tau_l) = x_d(j|i) \text{ and}$$

$x_d(j+1|i) = x_d(N_{sub}\tau_s + (j+i)\tau_l | i\tau_l)$ and where $\bar{F}(\cdot)$ represents a discretization of the differential Equation (1) with sampling time τ_s . The prediction horizon is defined as $N = (t_f - t_0)/\tau_l$. In

the remainder of this subsection, the selection of the sub-sampling factor N_{sub} and prediction horizon N are discussed. Then, the solver used to solve (20) is presented.

2.7.1. Subsampling factor N_{sub}

By increasing N_{sub} , τ_s will decrease such that $F(\cdot)$ in (20) will more accurately model the (continuous) behaviour of $f(\cdot)$ as in (1). However, the computation time of the problem will increase. This subsection presents a simulation experiment, different values for N_{sub} are used to analyze the trade-off between accurately describing the behaviour of the system and the computation time of the problem in (20).

To analyse the loss in accuracy when discretizing the trajectory, the (continuous) trajectory would have to be obtained from the system in (1). The characteristic greenhouse climate time scale is in the order of 15 min to 1 h, according to van Straten et al. (2000). For this analysis we assume that a simulation with $N_{sub} = 10$, resulting in a discretization interval of $\tau_s = \tau_l \cdot N_{sub}^{-1} = 900 \text{ s} \cdot 10^{-1} = 90 \text{ s}$, is accurate enough to provide reliable estimates of the solutions of the system in (1). The optimisation problem in (20) is solved and a control strategy is obtained and applied to the system in open-loop simulations with $N_{sub} \in \{1, \dots, 10\}$.

As the greenhouse climate states have the shortest time constant, the effects of a low N_{sub} and thus a long discretization interval is most visible in these variables. Figure 2 presents the resulting trajectories from the simulations. Note that the trajectories corresponding to $N_{sub} = 1$ have been left out for the sake of clarity, these resulted in near-unstable behaviour due to the long discretization interval. One can observe from Fig. 2 that the trajectories are close for $N_{sub} > 3$. The simulations with $N_{sub} < 10$, are compared to the simulation with $N_{sub} = 10$, the resulting root-mean-squared-errors (RMSE) are presented in the bottom row of Fig. 2. From Fig. 2, one can observe that the further decrease of RMSE for $N_{sub} > 4$, is small, therefore in this research we choose $N_{sub} = 4$, yielding a discretization interval for the state equation of $\tau_s = 900 \text{ s} \cdot 4^{-1} = 225 \text{ s}$.

2.7.2. Prediction horizon N

Intuitively, by increasing the prediction horizon N , better performance with respect to the objective function is obtained. However, the computation time of the problem (20) will increase. This subsection presents a simulation experiment, different values for the prediction horizon N are used to

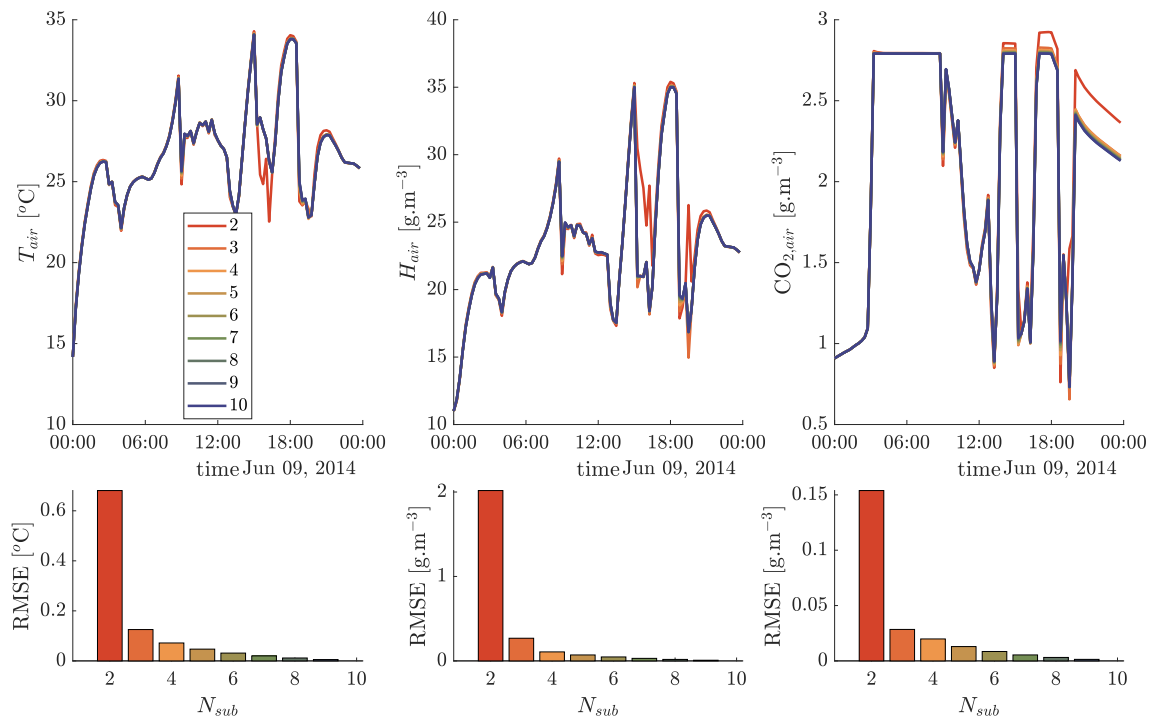


Fig. 2 – (top row) Greenhouse climate state trajectories for an input sequence applied to models with different subsampling intervals N_{sub} , values for inside temperature T_{air} , greenhouse air humidity H_{air} , and greenhouse air CO_2 concentration CO_2_{air} are presented. **(bottom row)** RMSE with respect to $N_{sub} = 10$ reference trajectory for the different subsampling intervals.

analyze the trade-off between suboptimality of the problem in (20) and the computation time.

Processes with slow time constants cause outputs to be affected by inputs for longer periods of time. According to [van Straten et al. \(2000\)](#), the greenhouse climate is characterised by a time constant in the order of 15 min to one hour (in open loop) and the time constant of a growing crop is in the order of weeks. Note that the inputs to a (near) pure integrator (in open loop) affect the output for a (near) infinite period. The fully-grown crop as described in subsection 2.5, is not a (near) pure integrator. First, the fact that the LAI_{max} is attained and is kept (close to) constant through leaf pruning, through control, lowers the time constant of the leaf buffer C_{leaf} . Second, the fruit development as described in [Vanhoor \(2011\)](#) is omitted, unripe fruit is sold after being partitioned, removing this delay. Third, the temperature sum is compared to a threshold to indicate the start of generative phase, for a fully grown crop this temperature sum will have exceed the threshold described in Vanhoor and the value of the temperature sum is obsolete.

To analyse the decrease in performance for a shrinking prediction horizon, the optimisation problem in (20) is solved for various values of N . Choosing a value of $N \gg 2 \cdot 96$, will ensure the effects of the inputs have diminished and the performance is (near) optimal, to this extent we choose $N = 6 \cdot 96 = 480$. [Figure 3](#) presents the optimised state trajectories for the greenhouse climate for $N \in \{96, 192, 288, 384, 480, 576\}$. For $N = 192$, one can observe coinciding trajectories for the first day of the simulation with the reference $N = 480$. The simulation studies presented in this paper use a prediction horizon of $N = 288$, which represents a length of 3 days. One can also observe the greediness of optimal control, the

controller does not consider what happens after the prediction horizon. After the last radiation in the horizon, the objective function cannot be impacted in a positive way for the remainder of the horizon, therefore the heating, CO_2 injection are switched off. Also, the leaves are harvested to minimise transpiration avoiding a heating demand to maintain the system within the constraints.

2.7.3. Solver

The optimisation problem in (20) is solved using the nonlinear optimisation software package IPOPT solver ([Wächter & Biegler, 2006](#)), with linear solver MA57 from HSL ([HSL, 2019](#)). The IPOPT solver is interfaced using CasADI ([Andersson et al., 2019](#)). Due to the multiple-shooting approach to solving the optimisation problem, the number of optimisation variables is $(n_u + n_x) \cdot N$, with $n_u = 13$ and $n_x = 8$ the number of inputs and states. With a prediction horizon of three days and 15 minute discretization interval, $N = 96 \cdot 3$, yielding 6048 variables to be optimised. The combination of IPOPT with CasADI allows an efficient solving process of this problem, as CasADI provides Jacobian and Hessian information to the IPOPT solver ([Andersson et al., 2019](#)).

2.8. Rule-based controller

In order to be able to validate the models and their interconnection, a control strategy is designed resembling KWIN ([Vermeulen, 2016](#), p. 330) and therefore the state-of-the-practice. To this effect a rule-based controller is employed. The ventilation rules are based on [Vanhoor et al. \(2011\)](#). Key features of this rule-based controller are:

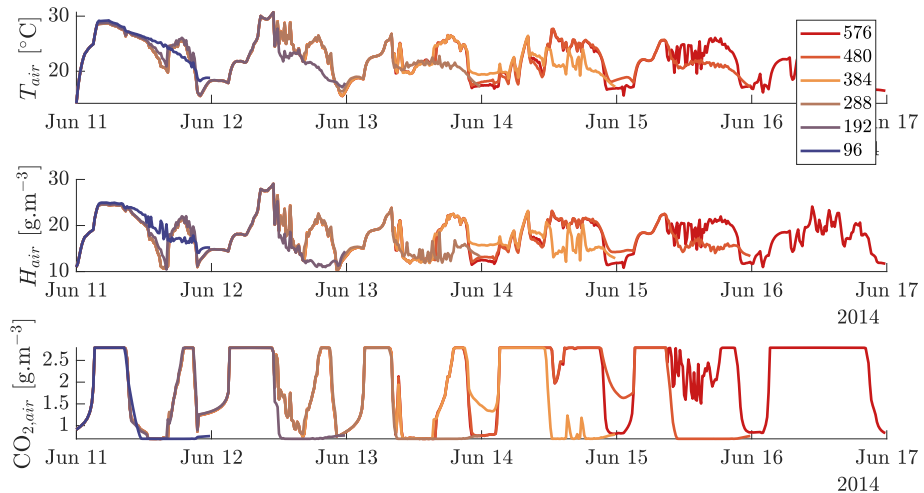


Fig. 3 – Optimal trajectories for greenhouse air temperature T_{air} , greenhouse air humidity H_{air} and greenhouse air CO_2 concentration $CO_{2,air}$ for different values of the prediction horizon N , here $N \in \{96, 192, 288, 384, 480, 576\}$.

- lamps are on from 2:00 to 18:00, except when instantaneous global radiation exceeds 600 W.m^{-2} or when the predicted radiation sum exceeds $14 \text{ MJ.m}^{-2}.\text{day}^{-1}$.
- greenhouse air temperature setpoint is 19.5°C while lamps are on or radiation from the sun is present, 18.5°C otherwise. The setpoint is maintained using a P-controller.
- CHP is on when lamps are on, unless heat cannot be directed to the greenhouse or to the buffer. Only after the heat buffer depleted, a heating demand switches on the CHP. Excess electricity produced by CHP is sold.
- CO_2 setpoint is 1000 ppm (1.83 g.m^{-3} at 20°C), controlled by a P-controller. If more CO_2 is produced by the CHP and/or buffer than required, the surplus is injected.
- the ventilation is forced to close if greenhouse air temperature is 1°C below temperature setpoint. The ventilation opens when greenhouse air relative humidity exceeds 85 %. Both ventilation incentives are P-controlled.
- Screens are closed if outdoor temperature is below 5°C during the day or 10°C during the night. The screens open when ventilation is required.

2.9. KWIN

The *Kwantitatieve Informatie voor de Glastuinbouw* (KWIN) (Vermeulen, 2016, p. 330) periodically summarises actual information on Dutch greenhouse horticulture. Aside from other relevant horticultural information, it also contains reference operational figures, such as crop yield, gas use and electricity use. The information from the KWIN will be used in this research as a representation of the state-of-the-practice. The operational figures used in this research are those for a greenhouse with truss tomatoes, planted in week 42, with a CHP and with HPS lighting, specifically budget G56. To be able to compare the performance of the

controlled greenhouse system here, the costs (16) and contributions to the carbon footprint (19) of all inputs are taken from the KWIN, these have been summarised in Table 3. Also, the limitations of the control inputs, presented in Table 2, have been adopted from KWIN. The remainder of this subsection will state some remarks with respect to the use of the KWIN.

The crop price provided in the KWIN is the price that is required to reach the break-even point. The resulting crop price does reflect the seasonal differences. As the KWIN will be used to compare the results to the state-of-the-practice, the crop price from the KWIN is adopted. To mitigate the inaccuracy due to not including fruit growth in the crop model, as discussed in subsection 2.5, the crop price from the KWIN is shifted 30 days forward in time. The assimilates partitioned to the fruits are sold at that time instance for the price of 30 days later. Also, the KWIN is based on the average prevailing weather during a year. The simulations in this paper are based on weather data, the source of which is presented in subsection 2.10.

2.10. Weather data

The uncontrollable inputs d represent the outside weather variables, namely: global radiation sum Q_{sun} , outside temperature T_{out} , outside CO_2 concentration $CO_{2,out}$, outside absolute air humidity H_{out} and wind speed v_{wind} . The data is measured at 5 min interval, for the years 2011–2014, although only year 2014 is used in this research. The weather data originates from an experiment described in Kempkes et al. (2014), where various energy-saving options in greenhouses were investigated in a Venlow Energy kas located in Bleiswijk, The Netherlands. The daily global radiation sum Q_{sun}^D , outside temperature T_{out} , outside absolute air humidity H_{out} , wind speed v_{wind} are presented in Fig. 4. The areas in Fig. 4 that envelop the lines indicate the daily variation (maximum and minimum) of the variable, except for the global radiation which is expressed as a daily sum. Note, that only the weather data is used, the parameters of the greenhouse and the experiment are not relevant here.

3. Results

To evaluate to what extent LED lighting improves the performance of an optimally controlled greenhouse system, several simulation studies are performed. The first simulation study encompasses a simulation over an interval of 218 days with generative crops. These simulations are performed for a greenhouse equipped with HPS lighting, LED lighting and no lighting, all controlled using the optimal control algorithm presented in subsection 2.7. Also, a greenhouse equipped with HPS lighting is simulated when controlled using the rule-based controller presented in subsection 2.8. The results of this simulation study are presented in subsection 3.1. In subsection 3.2, the optimally controlled system is simulated for four 7-day intervals, using the different quantisation step sizes as discussed in subsection 2.3.

3.1. Season simulations

The operation of the controlled greenhouse system is simulated for a period of 218 days, from the 11th of January to the 16th of August. The start of the simulation period is offset compared to the period in which data is available in the KWIN. This is due to (a) the unavailability of weather data, see subsection 2.10 and (b) the requirement for a fully-grown, producing crop introduced in subsection 2.7.2. To ensure the state of the system in the simulations here at the 11th of January reflects the state of the system at the 11th of January in the KWIN, the state is estimated through simulations with the crop model as presented in [Vanhoor \(2011\)](#) using the same planting date. The end of the simulation period is advanced to the 16th of August as the crop growth and transpiration model presented in subsection 2.5 does not predict the behaviour of a topped tomato crop. As [Vermeulen \(2016, p. 330\)](#) does not detail the topping of the crop, the crop is assumed to be topped 4 weeks prior to the end of the cropping cycle.

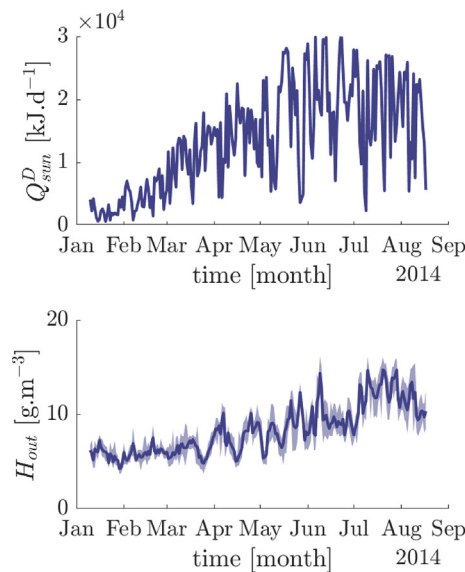


Fig. 4 – The weather data input to the uncontrollable inputs of the greenhouse system d during the simulations presented in this paper. (left-to-right, top-to-bottom) The daily global radiation sum Q_{sun}^D , outside temperature T_{out} , outside absolute air humidity H_{out} and wind speed v_{wind} .

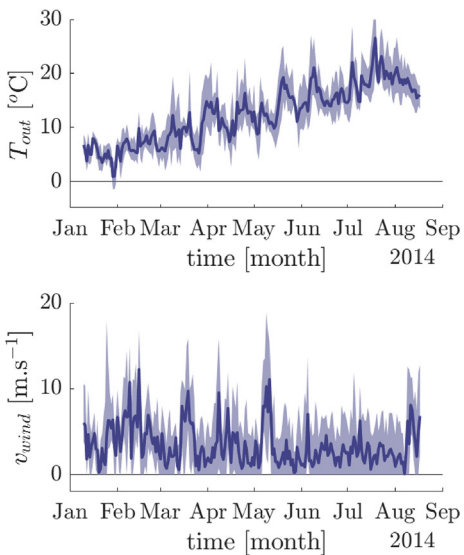
In practice, the integration of a lighting systems might be coupled to a different configuration of the system, e.g. larger heat buffer and/or larger CHP. The simulations studies presented in this paper apply to a greenhouse which is characterised by the parameterisation of the chosen models and the systems those models have been validated with. In the simulations presented here only the lighting system changes.

For the sake of clarity and direct comparison with the 4-week average of KWIN, the 4-week average value of all relevant signals will also be plotted, using the same averaging intervals as in KWIN. The 4-week average values of a simulation denoted by, e.g., OC is $PA(\text{OC})$ (periodic average).

For the sake of clarity, the results of the six simulations are split into two sets. In subsection 3.1.1, the simulations with the greenhouse system with HPS lighting controlled by the rule-based controller and the optimal control algorithm are presented along with relevant data from the KWIN. The second set, presented in subsection 3.1.2, presents the simulations with the optimal control algorithm in (20) for a greenhouse system with LED lighting, HPS lighting or no lighting installed.

3.1.1. Set 1: rule-based control, optimal control and KWIN

The yearly totals of the operational return J for the three simulations in the first set are presented in [Table 4](#), along with the components that determine its value through (16), i.e. crop harvest u_{frt} , gas use by the CHP s_{chp} , gas use by the boiler s_{boi} , (pure) CO_2 bought u_{cby} , electricity sold u_{ese} and electricity bought u_{eby} . The carbon footprint p_2 , according to (19), is presented in the last column of [Table 4](#). One can observe the highest operational return in the simulation with the optimal controller OC, $65.14 \text{ euro.m}^{-2}$, an increase of 6.18 euro.m^{-2} (+10 %) with respect to the date in KWIN. The simulations with the rule-based controller, Rule, realised the worst operational return, a decrease of 9.78 euro.m^{-2} (–17 %) with respect to the date in KWIN. The high operational return of the simulation



with the optimal controller OC can be explained by the higher fruit harvest u_{frt} , 12.54 kg.m^{-2} (+19 %) with respect to the date in KWIN. From the unit prices in [Table 3](#), one can observe that fruit harvest contributes considerably to the operational return, inducing the difference between the data from KWIN and simulations with OC. To achieve this increased fruit harvest, the optimal controller OC uses $5.64 \text{ m}^3 \cdot \text{m}^{-2}$ more gas (+ 14 %) compared to KWIN. The rule-based controller uses the least amount of gas but injects more CO_2 and therefore has to buy considerably more CO_2 than is used in the other simulations. Also the price of buying (pure) CO_2 is considerable, $0.11 \text{ euro.kg}^{-1}$, resulting in a total expense of 1.62 euro.m^{-2} on bought CO_2 for the rule-based controller. The increased CO_2 bought by the rule-based controller compensates the decreased gas use when evaluating the carbon footprint p_2 , which is as high as the carbon footprint of the optimal controller.

To be able to analyse the seasonal differences, the daily sums of the combined gas use of the CHP and boiler s^D , electricity exchange with the grid $u_{eby}^D - u_{ese}^D$ and CO_2 bought u_{cby}^D are presented in [Fig. 5](#). One can observe that the increased yearly total gas used by the optimal controller as presented in [Table 4](#), is primarily due to an increased gas use throughout the period from May to August. The gas use throughout the season is similar for the simulations with the rule-based controller and the data from the KWIN. As the KWIN only provides a yearly total for the electricity exchange with the grid it cannot be compared on a seasonal timescale. One can observe, however, that the rule-based controller uses more electricity from the grid, especially in wintertime. As a CO_2 demand is not coupled to the level of operation of the CHP u_{chp} and boiler u_{boi} in the rule-based controller, the rule-based controller has to buy CO_2 for injection throughout a significant part of the season in which the CHP is used less. The daily sum of fruit harvest for the three simulations in the first set is presented in [Fig. 6](#). One can observe in [Fig. 6](#) that the difference in fruit harvest presented in [Table 4](#) between KWIN and OC results from an increased fruit harvest throughout most of the season, most notably during March and April. Also, in [Fig. 6](#) one can observe that the daily sums of the rule-based controller and the KWIN are similar throughout the season. The daily sum of the p_1 performance for the three simulations in this set is presented in [Fig. 7](#). The effect of the decreasing crop prices c_{frt} throughout summer is clearly visible. The latter induces the decrease in the difference in p_1 -performance throughout summer even though the crop yield in the simulations with OC are higher throughout summer.

The sudden decrease and subsequent increase of crop growth at the 13th of June is found to be due to an increase in the fruit price c_{frt} , 30 days later, 13th of July. The controller chooses to harvest less fruits before the 13th of June, such that more fruits can be sold after the 13th of June. The latter is comparable to a grower that, knowing a price increase is expected in the near future, will try to postpone harvesting as much as possible.

3.1.2. Set 2: No lighting, HPS lighting and LED lighting

The yearly totals of the operational return J for the three simulations in the second set are presented in [Table 5](#) which is structured similar as [Table 4](#). The simulation with HPS discussed here is the same as the one in the first set, where it was denoted by OC. One can observe that the operation return J for the LED-equipped greenhouse is 6.28 euro.m^{-2} higher (+9 %) with respect to the HPS-equipped greenhouse. [Table 5](#) shows that the biggest difference between both simulations is the electricity exchange with the grid. The LED-equipped greenhouse buys 24.34 kWh.m^{-2} and sells 64.00 kWh.m^{-2} , the HPS-equipped greenhouse buys 71.86 kWh.m^{-2} more and sells 16.39 kWh.m^{-2} less electricity. This results in a net difference of 88.51 kWh.m^{-2} , note, however, that buying and selling electricity are not weighted with the same factor to arrive at operational return, i.e. $c_{ese} \neq c_{eby}$, see [Table 3](#). The resulting difference expressed in monetary units, after multiplication with c_{ese} and c_{eby} , indicates a 3.60 euro.m^{-2} difference. The different electricity consumption accounts for 57 % of the difference in operational return between the HPS and LED-equipped greenhouse. The latter also affects the carbon footprint, the LED-equipped greenhouse has a footprint which is 41.09 kg.m^{-2} lower, a decrease of 30 % compared to the HPS-equipped greenhouse. Other differences can be observed in the use of the boiler, s_{boi} , although this difference is rather low compared to the use of the CHP. Both greenhouses harvest a similar amount of fruits, the LED-equipped greenhouse harvests 2.58 kg.m^{-2} more, an increase of 3 % compared to the HPS-equipped greenhouse. The lowest operational return is obtained for the greenhouse without artificial lighting No, which achieves $15.13 \text{ euro.m}^{-2}$ less (– 23 %) with respect to the HPS-equipped greenhouse. As the greenhouse without artificial lighting No uses a similar amount of gas as the HPS-equipped greenhouse, most of the resulting energy can be sold, selling 96.42 kWh.m^{-2} more than HPS, an increase of 202 %, resulting in a low carbon footprint. The greenhouse without artificial lighting No, emits the least CO_2 equivalents per produced kilo of tomatoes 0.19 kg.kg^{-1} , the HPS and LED –

Table 4 – The yearly sums of the operational return J , crop harvest u_{frt} , gas use by the CHP s_{chp} , gas use by the boiler s_{boi} , (pure) CO_2 bought u_{cby} , electricity sold u_{ese} , electricity bought u_{eby} and carbon footprint p_2 for the three simulations in the first set. The first set encompasses simulations with the rule-based controller, denoted by Rule, the optimal controller, denoted by OC, and the respective data in the KWIN.

	J [euro.m $^{-2}$]	u_{frt} [kg.m $^{-2}$]	s_{chp} [m $^3 \cdot \text{m}^{-2}$]	s_{boi} [m $^3 \cdot \text{m}^{-2}$]	u_{cby} [kg.m $^{-2}$]	u_{ese} [kWh.m $^{-2}$]	u_{eby} [kWh.m $^{-2}$]	p_2 [kg.m $^{-2}$]
Rule	49.18	64.63	31.90	0	14.72	18.38	93.39	135.80
KWIN	58.96	67.46		39.21	0	39.42	101.54	130.90
OC	65.14	80.00	44.78	0.07	0.0019	47.61	96.52	135.53

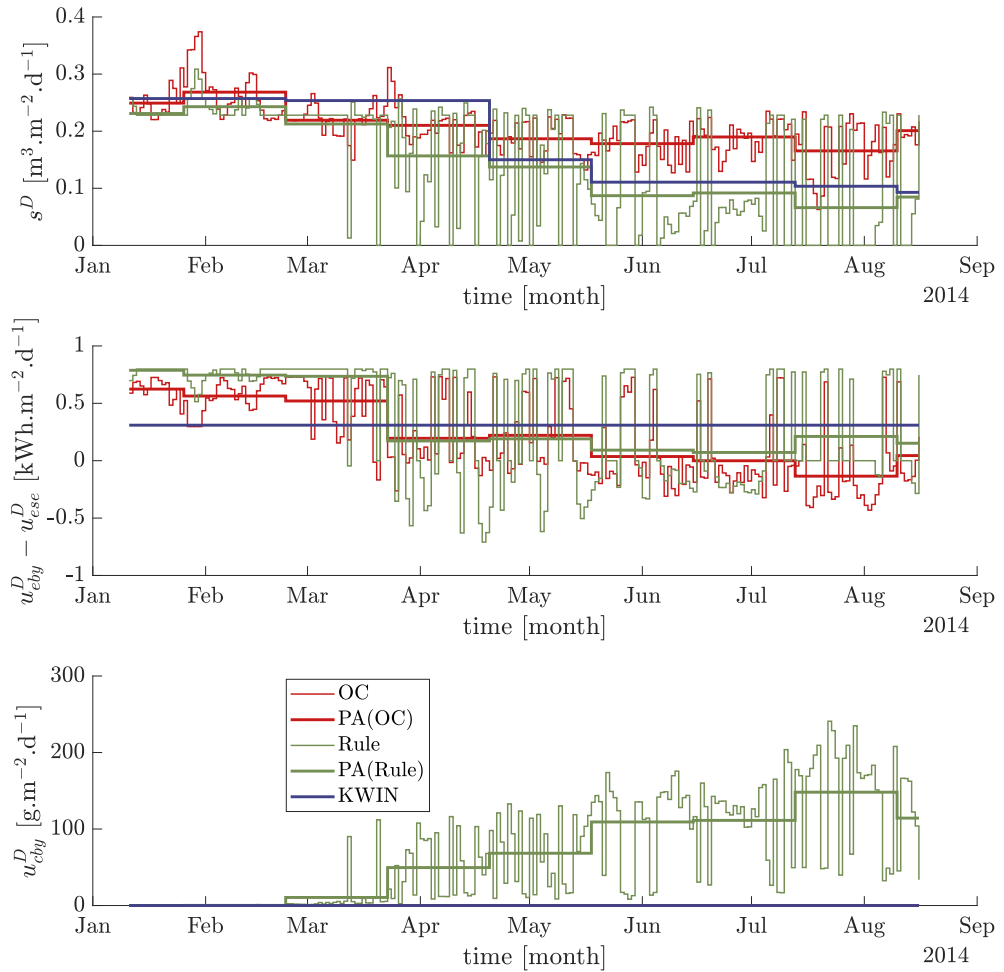


Fig. 5 – The daily sums of the (top) gas use s^D , (middle) electricity exchange with the grid $u_{eby}^D - u_{ese}^D$ and (bottom) pure CO₂ bought u_{cby}^D for simulations with the controlled greenhouse. Rule denotes the simulations with rule-based controller, as presented in subsection 2.8. OC denotes the simulations with the optimal controller, presented in subsection 2.7. The latter simulations are compared to the data from the KWIN, denoted by KWIN. PA(·) is used to denote the 4-week average of the daily signals.

equipped greenhouse achieve 1.69 kg.kg⁻¹ and 1.14 kg.kg⁻¹, respectively.

To be able to analyse the seasonal differences in the second set, the daily sums of the combined gas use of the CHP and boiler s^D , electricity exchange with the grid $u_{eby}^D - u_{ese}^D$ and CO₂ injection u_{cby}^D are presented in Fig. 8. One can observe in the top panel of Fig. 8 that the increased gas use of the LED-equipped greenhouse mainly results from the winter period. During this period, January to April, the LED-equipped greenhouse sells more electricity to the grid as compared to the HPS-equipped greenhouse, the latter buys considerable amounts of energy in this period. This indicates that it does not pay off for the HPS-equipped greenhouse to generate the electricity itself, possibly due to a heat demand. Where both the HPS and LED-equipped greenhouse use the energy to power the artificial lighting,

the greenhouse without artificial lighting No sells all the produced electricity as by product of the heat demand. From the bottom panel of Fig. 8, one can observe that the reduced gas use of the HPS-equipped greenhouse does result in a small increase in (pure) CO₂ bought u_{cby}^D . To be able to analyse these seasonal differences on a more detailed level, Fig. 9 presents optimised trajectories for artificial lighting u_{hps} and u_{led} , CHP level of operation u_{chp} , electricity exchange with the grid $u_{eby} - u_{ese}$, inside and outside temperature T_{air} and T_{out} and CO₂ concentration $CO_{2,air}$ for January 12th and June 20th. In the winter season, January 12th, the LED-equipped greenhouse also operates the CHP at night, resulting in more electricity sold to the grid. One can observe that the temperature T_{air} , however, is not significantly different, the CO₂ concentration $CO_{2,air}$ is considerably different at night, however. In the summer season, June

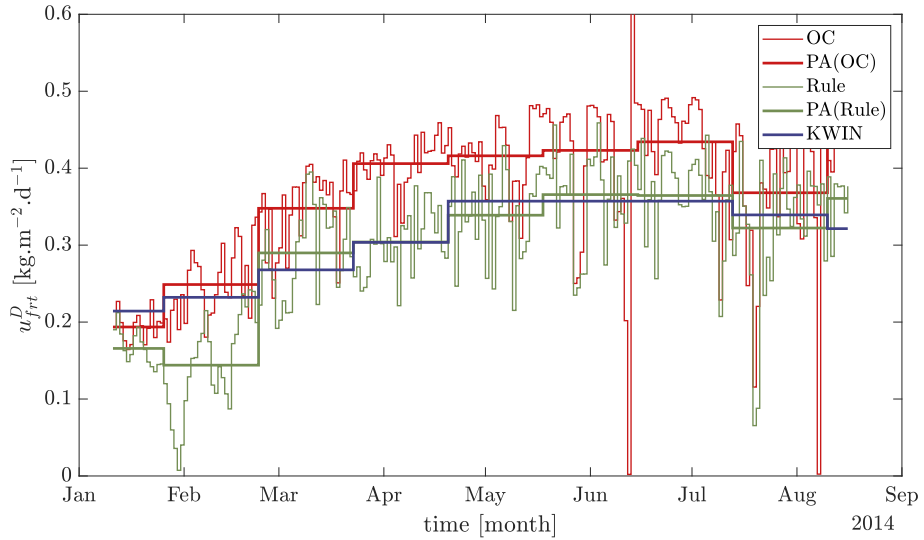


Fig. 6 – The daily sum of the fruit harvest u_{frt}^D for simulations with the controlled greenhouse. Rule denotes the simulations with rule-based controller, as presented in subsection 2.8. OC denotes the simulations with the optimal controller, presented in subsection 2.7. The latter simulations are compared to the data from the KWIN, denoted by KWIN. PA() is used to denote the 4-week average of the daily signals.

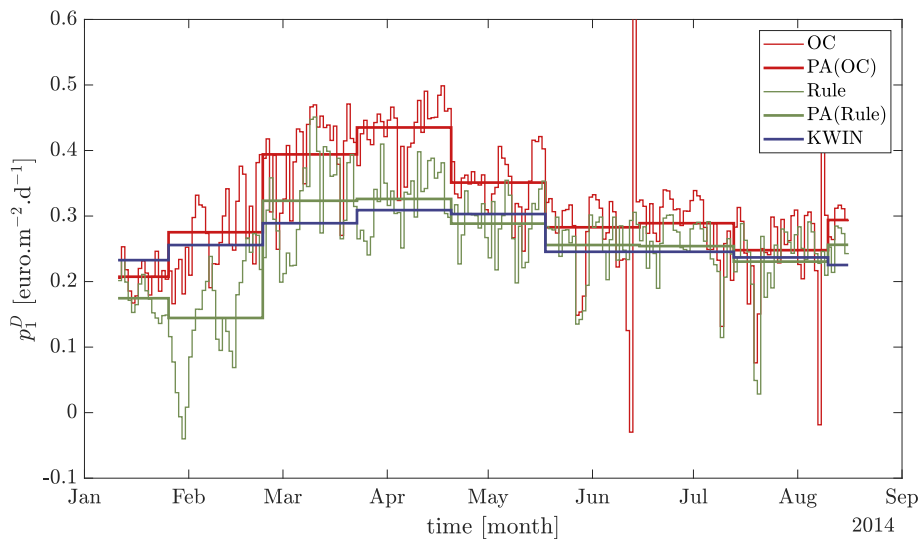


Fig. 7 – The daily sum of the p_1 -performance p_1^D for simulations with the controlled greenhouse. OC denotes the simulations with rule-based controller, as presented in subsection 2.8. Rule denotes the simulations with the optimal controller, presented in subsection 2.7. The latter simulations are compared to the data from the KWIN, denoted by KWIN. PA() is used to denote the 4-week average of the daily signals.

Table 5 – The yearly sums of the operational return J , crop harvest u_{frt} , gas use by the CHP s_{chp} , gas use by the boiler s_{boi} , (pure) CO_2 bought u_{cby} , electricity sold u_{ese} , electricity bought u_{eby} and carbon footprint p_2 for the three simulations in the second set. The second set encompasses simulations with the optimal controller for a greenhouse equipped with HPS lighting, LED lighting and No lighting.

	J [euro.m $^{-2}$]	u_{frt} [kg.m $^{-2}$]	s_{chp} [m $^3.m^{-2}$]	s_{boi} [m $^3.m^{-2}$]	u_{cby} [kg.m $^{-2}$]	u_{ese} [kWh.m $^{-2}$]	u_{eby} [kWh.m $^{-2}$]	p_2 [kg.m $^{-2}$]
HPS	65.14	80.00	44.78	0.07	0.0019	47.61	96.52	135.53
LED	71.24	82.58	50.95	0.38	0.0019	64.00	24.34	94.47
No	50.01	57.05	40.93	0.30	0.0018	144.03	0.10	10.63

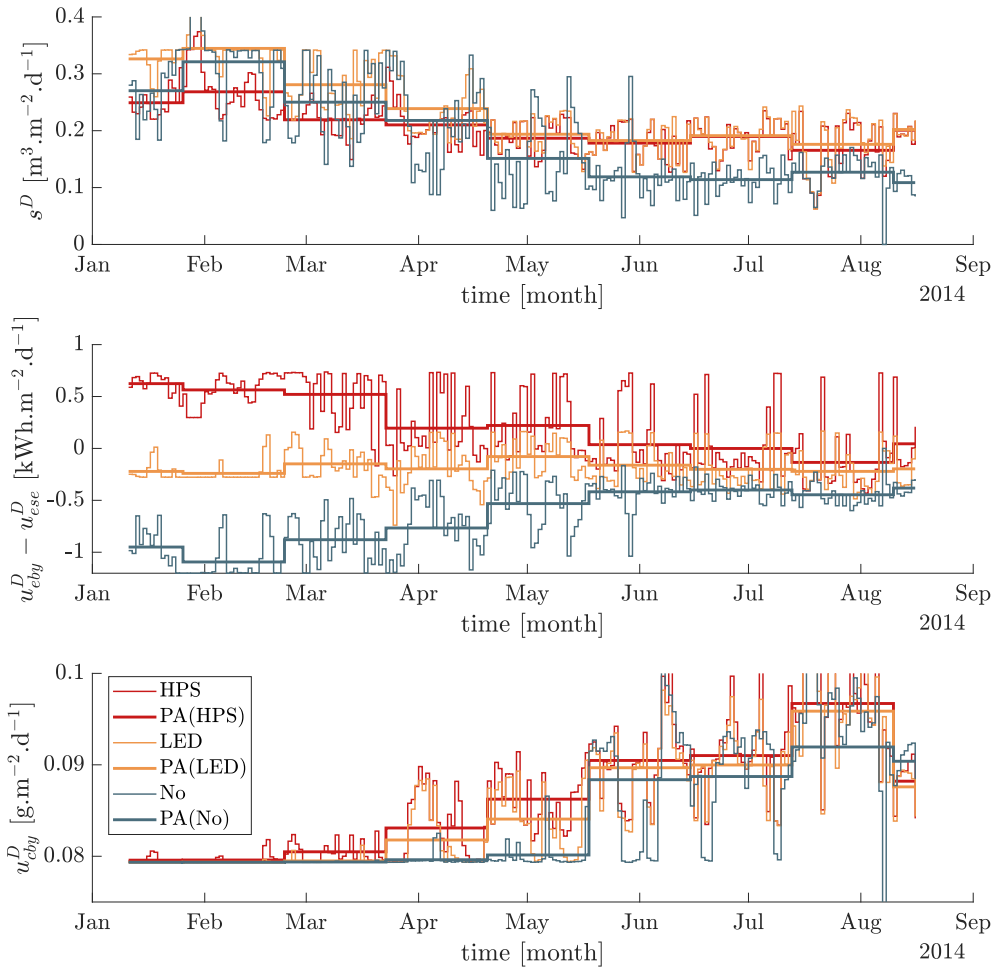


Fig. 8 – The daily sums of the (top) gas use s^D , (middle) electricity exchange with the grid $u_{eby}^D - u_{ese}^D$ and (bottom) pure CO₂ bought u_{eby}^D for simulations with the controlled greenhouse. The HPS-equipped greenhouse is denoted by HPS, the LED-equipped greenhouse is denoted by LED and the greenhouse without artificial lighting is denoted by No.

20th, the artificial lighting is not employed throughout the entire day as compared to January 12th. The latter effect causes the differences between resource use of the HPS and the LED-equipped greenhouse, as presented in Fig. 8.

The daily sum of fruit harvest for the three simulations in this set is presented in Fig. 10. One can observe in Fig. 10, that, all throughout the season, the LED-equipped greenhouse achieves a higher fruit harvest as compared to the HPS-equipped greenhouse, which supports the figures in Table 5. The added fruit harvest through artificial lighting is largest throughout the winter season, as can be observed by comparing the both greenhouse with artificial lighting to the one without. The daily sum of the p_1 performance for the three simulations in this set is presented in Fig. 11. One can observe, similar as in Fig. 7, that due to decrease fruit prices c_{frt} the added benefit of the increase in crop harvest becomes smaller. However, the CHP is operated less in the summer season, less energy is sold as can be observed in Fig. 8 and that all three greenhouse operate more alike as compared to the winter season.

3.2. Simulations with quantisation effects

To quantify the effect of quantisation in the system, as referred to in subsection 2.3, the optimised trajectories u_{hps}^* and u_{led}^* are quantised to on-off signals, referred to as $\Delta = 1$, and to signals with four possible values, referred to as $\Delta = 0.33$. The value Δ is here referred to as the quantisation step size. After quantisation the trajectory for u_{hps}^* or u_{led}^* is fixed and the optimization algorithm in (20) is used to optimise the other control inputs. The latter approach ensures that the imposed constraints are satisfied also after the quantisation has been applied. The three different quantisation strategies have been applied in simulations with three different lighting systems over the course of four 7 – day periods in January, April, June and August. For the simulations without a lighting system no quantised signals have to be applied. The state of the system at the first day in the interval is based on the state of the system at the specific day in the simulations with HPS lighting in subsection 3.1.

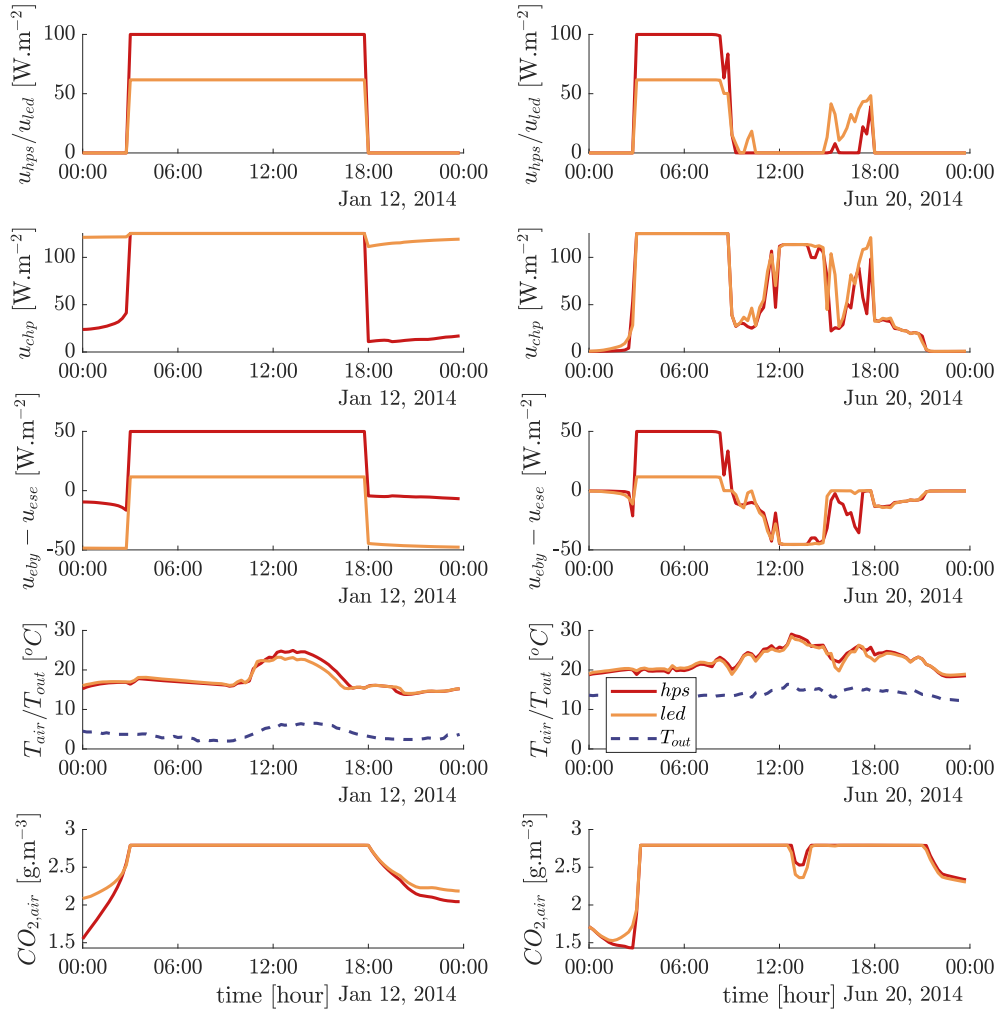


Fig. 9 – Relevant control trajectories for simulations with the LED-equipped greenhouse and HPS-equipped greenhouse during January 12th (left) and June 20th (right). Plotted are (row 1) artificial lighting u_{hps} and u_{led} , (row 2) CHP level of operation u_{chp} , (row 3) electricity exchange with the grid $u_{eby} - u_{ese}$, (row 4) greenhouse air and outside temperature T_{air} and T_{out} , (row 5) greenhouse air CO_2 concentration $\text{CO}_{2,air}$.

The average operational return for the resulting seven-day simulations are presented in Table 6. One can observe that the quantisation step size does not significantly affect the average operational return in the intervals tested here. The algorithm with a lower quantisation step size can produce the same trajectories as the next increased level of quantisation step size, i.e. the trajectories denoted by u^* in Table 6 can be exactly the same as those denoted by $\Delta = 1/3$. Note, therefore, that the increase in average operational return going from $\Delta = 1/3$ to $\Delta = 1$ for a LED-equipped greenhouse in April and the increase from u^* to $\Delta = 1/3$ result from numerical inaccuracies in the solution of the optimisation algorithm in (20). Figure 12 presents the original and quantised trajectories for April 15th for both an HPS and LED-equipped greenhouse. One can observe how quantisation will typically result in a value lower or higher. The original trajectories indicate the optimal trajectory, if through quantisation more power is directed to the light, this will reduce the operational return.

4. Discussion

In this section, the results of the simulation studies presented in section 3 are discussed in the context of the main question of this paper: to what extent does LED lighting improves the performance of an optimally controlled greenhouse system, measured in operational return and carbon footprint. Subsection 4.1 discusses the validation of the interconnection of the models presented in subsection 2.2, 2.3, 2.4 and 2.5. The performance of the optimal controller based on (20) is compared with respect to the state-of-the-practice, here KWIN, and the rule-based controller in subsection 4.2. Subsection 4.3 discusses the observed differences between an HPS and LED-equipped greenhouse, answering and discussing the main question of this paper. The effect of quantisation in the context of the estimated performance increase from subsection 4.3 is discussed in subsection 4.4.

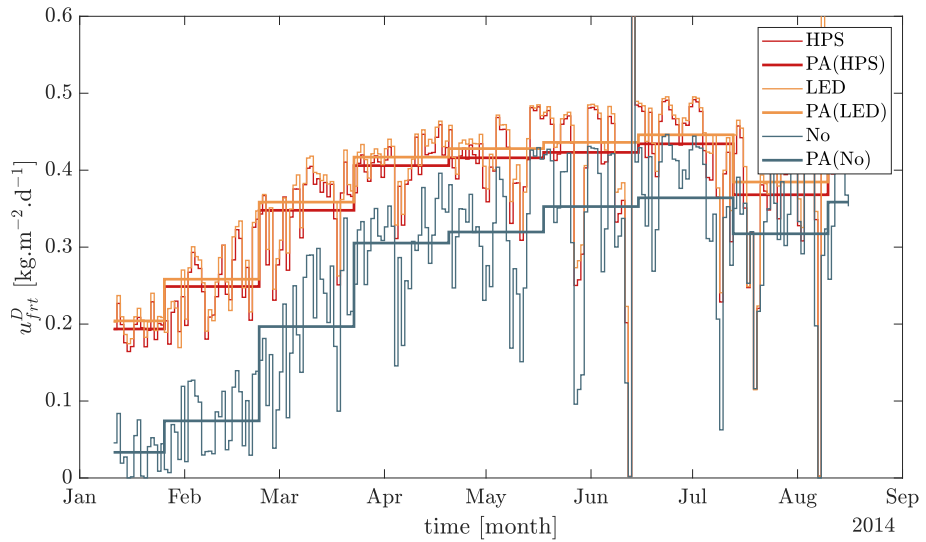


Fig. 10 – The daily sum of the crop yield u_{frt}^D of the HPS-equipped greenhouse, denoted by HPS, the LED-equipped greenhouse, denoted by LED and the greenhouse without artificial lighting, denoted by No. PA (•) is used to denote the 4-week average of the daily signals.

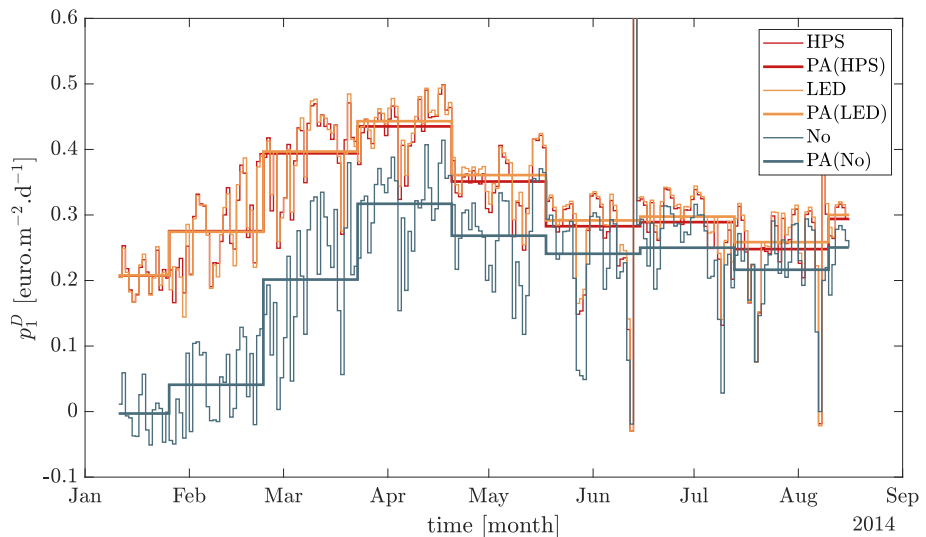


Fig. 11 – The daily sum of the p_1 -performance p_1^D of the HPS-equipped greenhouse, denoted by HPS, the LED-equipped greenhouse, denoted by LED and the greenhouse without artificial lighting, denoted by No. PA (•) is used to denote the 4-week average of the daily signals.

4.1. Model validation

The parts of the model presented in subsection 2.2, 2.3, 2.4 and 2.5 have already been validated in their respective publications. This subsection will, therefore, discuss the validation of the interconnection of the parts of the model, instead of the separate models and will therefore focus on the performance indicators presented in subsection 2.6. The concept of model validation has different meanings in different disciplines (Eker et al., 2018). Here, we use the term in the sense of having “usefulness with respect to some purpose [...] and suitability for its intended use” (Eker et al., 2018). The model will be validated using data from the KWIN. Since KWIN provides

Table 6 – The average operational return J (€.m^{-2}) per day in the seven-day interval for January, April and June. For each interval No lighting, HPS lighting and LED lighting are compared using two quantisation step sizes, i.e. $\Delta = 1$ and $\Delta = 1/3$.

	Jan			Apr			Jun		
	No	HPS	LED	No	HPS	LED	No	HPS	LED
u^*	0.04	0.16	0.21	0.31	0.35	0.37	0.17	0.19	0.20
$\Delta = 1/3$		0.15	0.20		0.35	0.36		0.19	0.21
$\Delta = 1$		0.15	0.20		0.35	0.37		0.19	0.20

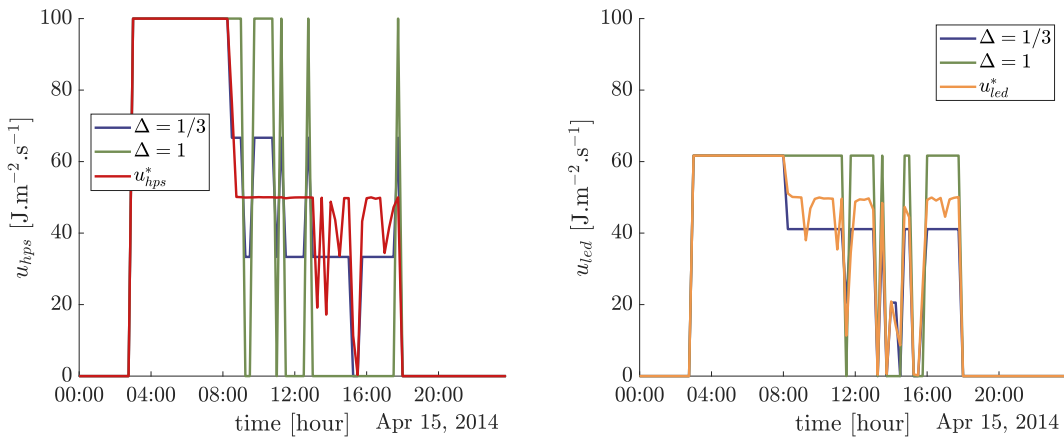


Fig. 12 – Original and quantised trajectories for 15th of April, for both the HPS-equipped greenhouse (left) and LED-equipped greenhouse (right). The continuous control inputs are denoted by u^*_{led} and u^*_{hps} . Resulting trajectories for a quantisation step size of $\Delta = 1$ and $\Delta = 1/3$ have also been depicted.

high-level numbers on the performance of a greenhouse in the state-of-the-practice, we believe that this data suffices for evaluating the interconnection of the parts of the model. The rule-based controller presented in subsection 2.8 arguably controls the greenhouse to a similar performance compared to the state-of-the-practice. Therefore, if the performance indicators of the simulation with the rule-based controller match those of the KWIN, the model describes the behaviour of the system in a way that is consistent with what is known about current practice, in terms of the performance indicators used in this study. As such, the model is deemed suitable for use in subsequent contributions presented in this section.

One can observe from the results presented in subsection 3.1.1 that the performance indicators of the simulation with the rule-based controller match those of the KWIN to a large extent. The total operational return of the greenhouse system controlled by the rule-based controller is 9.78 euro.m⁻² lower than the data from the KWIN. The overall resource use, as presented in Fig. 5 and the crop yield, presented in Fig. 6, show similar behaviour throughout the simulations. Some of the discrepancies may be caused by the differences in the prevailing weather conditions between the simulations with the rule-based controller and those used in the KWIN. The KWIN uses a typical meteorological year, the effects of different prevailing weather conditions are, therefore, hypothesised to affect the seasonal results but the yearly totals to a lesser extent. We conclude that the model describes the behaviour of the system sufficiently accurate for the subsequent contributions presented in this section.

By choosing the initial state of the system to reflect that of a fully-grown crop, the behaviour of the model can only be validated for that part of the season. It cannot be concluded whether the model also describes the vegetative phase of crop growth sufficiently accurate. The assumption of a fully-grown crop, however, affects only the state of the crop growth and transpiration model. Since these models are based on physiological principles that take crop growth processes (e.g. leaf area index) into account, we hypothesise that the model can

also be used to describe the vegetative phase of crop growth sufficiently.

4.2. Optimal control performance

In the results presented in subsection 3.1.1, an increase in operational return of 10 % was observed when comparing the greenhouse system controlled by the optimal controller to the data representing the state-of-the-practice in KWIN. By combining the various elements that make up the operational return J in Table 4 and the resource costs in subsection 2.9 we conclude that the difference is mainly induced by an increased crop yield. The optimal controller harvests 12.54 kg.m⁻² more fruit while using 5.57 m³.m⁻² more gas and exchanging 13.21 kWh.m⁻² net less electricity than the KWIN. The latter trade-off combined with a more efficient allocation of the resources is hypothesised to result in the increased operational return. The carbon footprint of the optimally controlled greenhouse is similar to that of the KWIN.

None of the simulations in subsection 3.1 or subsection 3.2 lead to a parameterisation of the optimisation algorithm in (20) for which the solver did not converge to a solution. As undesirable configurations of the greenhouse system are penalised through explainable white-box models into the economic objective function, the constraints can reflect the domain of the models. Due to the assumptions presented in subsection 2.7.2, the proposed optimisation algorithm in (20) and its configuration only apply to fully-grown, producing crops. In order to be able to apply receding horizon optimal control also in the case of a vegetative crop, i.e. the period in which the resource costs are not balanced by crop yield, one should resort to e.g. the time-scale decomposition as described in van Henten & Bontsema, 2009, in order for the optimisation algorithm to remain computationally feasible. As a non-producing crop will not balance the costs of resources through crop yield, in the case of a purely economic cost function, a long horizon, exceeding the length of the vegetative phase would be required.

Upon execution of the optimisation algorithm in (20), the actual and future prevailing weather d and actual and future crop price c_{frt} are input to the optimisation algorithm. In practice, however, the weather d cannot be predicted perfectly. The crop price c_{frt} in practice will also result from a prediction of the crop price 30 days into the future. Additionally, the simulated state of the system x_t is input to the optimisation algorithm in (20) upon execution. In practice, the state of the system will be the result of measurements with a limited accuracy, resulting in errors and uncertainty. The 10 % increase in operational return should therefore be seen as a performance bound, i.e. the performance that can be achieved if perfect predictions and measurements are available to the optimisation algorithm in (20).

Concluding, the optimal controller achieves a 10 % increase in operational return over part of the season that was simulated. The latter 10 %, however, does indicate a performance bound as perfect predictions of the weather and crop price as well as perfect measurements of the system are used here. The proposed approach is valid for greenhouses with fully-grown, producing crops.

4.3. Comparison of lighting systems

In the simulations presented in subsection 3.1.2, the LED-equipped greenhouse controlled by an optimal controller achieved an operational return which is 6.28 euro.m⁻² higher than an HPS-equipped greenhouse controlled by an optimal controller, an increase of 9 %. Also, the carbon footprint of the LED-equipped greenhouse is 30 % lower as compared to the HPS-equipped greenhouse, in the simulations presented here. The results of the simulations presented in Table 5, combined with the prices presented in subsection 2.9, show that this difference is for 57 % induced by a decreased electricity use of the LED-equipped greenhouse system. Cheaper electricity from the grid, a decreased c_{eby} , or a decreased sales price of electricity to the grid will mitigate the observed increase. Also, if the electricity from the grid is more sustainable, i.e. a lower γ_{eby} , as it e.g. would originate from renewable resources, the decreased carbon footprint will also be mitigated. Due to the mechanistic nature of the presented model, new additions to the heating or energy generation, such as geo-thermal energy, windmills and/or solar panels, can be changed in the proposed model.

The performance increase discussed here is obtained in simulations in which the control inputs result from the optimisation algorithm which aims to solely optimise the operational return. A lower carbon footprint, which is not the current aim of the optimal controller, could be added to the cost function by penalizing carbon emissions. Potentially, an even lower carbon footprint could be obtained, however, most likely at the expense of operational return.

The models used in this paper do not take into account the potential positive (e.g. increased dry mass partitioning to fruits) and negative (e.g. Botrytis cinerea resistance) spectral effects that LED light can have on crop physiology, for instance by supplying far-red light (Ji et al., 2019). However, it does allow for the future inclusion of these effects as the selected crop model is mechanistic (white box) and variables such as partitioning are explicitly modelled.

As the system assumes the crop is just producing and start simulating from that point on, no conclusions can be drawn on the potential benefits or drawback of using LED lighting in the vegetative phase of the crop. In order to add this to the proposed approach a solution as presented in subsection 4.2 would have to be added to the approach presented here.

4.4. Effect of quantisation on performance

The observed 9 % performance increases discussed above, when comparing optimal control to the state-of-the-practice and when comparing a LED-equipped greenhouse to one with HPS, assume that the artificial lighting can be dimmed, i.e. any value between 0 % and 100 % can be achieved. In practice, as explained in subsection 2.3, this cannot be achieved. Based on the results presented in subsection 3.2 we hypothesise that the effect of the quantisation in the system on this performance increase will not be significant if the optimisation algorithm is executed once more after quantisation. In Table 6, one can observe that the decrease in average operational return is not significant when various quantisation step sizes are used.

Removing the optimisation step after quantisation could lead to constraint violation, e.g. the optimal controller might find an optimum at 80 % power at a specific time instant, the 100 % power after quantisation, however, might increase the temperature such that it violates the constraint. As the aim of this research was to find to what extent it would change the performance of the greenhouse, no computationally optimal method was employed. A viable way to solve an optimisation algorithm as in (20) with the effects of quantisation included would be with employing an mixed-integer non-linear optimisation problem solver, as is used in van Beveren et al. (2019) to optimise the operation of boiler and CHP.

5. Conclusions & recommendations

The aim of this simulation study is to quantify the difference in operational return and carbon footprint in simulations using an optimally controlled greenhouse with HPS and LED lighting. To this extent, existing models in literature have been combined to arrive at a model of the greenhouse system. As the components have been validated in their respective publication, the interconnection of the models was validated using data representing the state-of-the-practice. An optimal control algorithm is proposed which, in combination with the aforementioned model, can control the greenhouse system using a purely economic cost function (no penalty functions). The simulations in this paper suggest a performance increase of 10 % in the operational return when comparing an optimally controlled greenhouse to the state-of-the-practice. Using the optimal control algorithm, the simulations presented here suggest an 9 % increase in operational return when comparing a greenhouse with HPS to one with LED lighting. Due to decreased electrical energy demand and an increased sale of electricity generated by a CHP in the greenhouse with LED lighting compared to HPS lighting, the simulations suggest a 30 % decrease in carbon footprint when adopting LED lighting systems, for tomatoes cultivated in

Dutch weather conditions. Simulations suggest that the effect of quantisation in the system, as the lamps can only be on or off, is not considerable.

The optimal controller here is configured using perfect predictions of the weather and crop price as well as perfect measurements of the system are assumed. The 10 % increase in operational return due to the integration of optimal control should be viewed as a theoretical bound on the performance increase. To the best of our knowledge the effect of the uncertainty inherited in predictions and models on the performance of the greenhouse system is unknown.

Declaration of competing interest

The authors declare the following financial interests/personal relationships which may be considered as potential competing interests: Authors W. Kuijpers, D. Katzin, R. van de Molengraft, and S. van Mourik are part of the research program LED it Be 50% with project number 14217, which is supported by the Netherlands Organisation for Scientific Research (NWO), LTO Glaskracht, Signify, Ridder Growing Solutions and B-Mex. Note, however: the supporting companies/institutions had no role or influence in the design and conduct of the study; collection, management, analysis, and interpretation of the data; preparation, review, or approval of the manuscript; and decision to submit the manuscript for publication.

Acknowledgment

Authors W. Kuijpers, D. Katzin, R. van de Molengraft, and S. van Mourik are part of the research program LED it Be 50% with project number 14217, which is supported by the Netherlands Organisation for Scientific Research, LTO Glaskracht, Signify, Ridder Growing Solutions and B-Mex. We would also like to thank the reviewers for the constructive feedback to improve the quality of this paper.

Appendix A. Heat Buffer Model

The model for the greenhouse heat buffer is taken from Seginer et al. (2018), it is represented by the differential equation

$$\dot{x}_s = u_{sto} - H_a, \quad (22)$$

where $x_s (J.m^{-2})$ represents the energy stored in the buffer, $u_{sto} (W.m^{-2})$ the energy supplied to and released from the buffer, see Table 2. The thermal losses are represented by $H_a (W.m^{-2})$, see (3). In (3), the value $\alpha (s^{-1})$ represents the thermal insulation of the heat buffer, this is given by.

$$\alpha = \frac{k_A \cdot s_A}{m_w \cdot c_w \cdot d_A}, \quad (23)$$

where $k_A (J.m^{-1}.s^{-1}.K^{-1})$ represents the thermal conductivity of the heat buffer surface, this has been chosen as $1.28 W.m^{-1}.K^{-1}$ equal to concrete. The surface area of the heat buffer $s_A = 309.81 (m^2)$ and mass of the water $m_w = 3.98 \cdot 10^5 (kg)$, have

been chosen based on a heat buffer with a height of $5.68 m$ and a radius of $4.73 m$, using the same ratio as in van Steekelenburg et al. (2011, p. 23), but matching the heat capacity of the heat buffer from Seginer et al. (2018). The maximum water temperature has been chosen $90 ^\circ C$, the lowest temperature $40 ^\circ C$. Using the heat capacity of water $c_w = 4182 (J.kg^{-1}.K^{-1})$, the energy for an empty heat buffer is $x_{s,off} = 40 \cdot c_w \cdot m_w = 1.67 \cdot 10^6 (J)$. The thickness of the heat buffer wall was chosen $d_A = 0.6 m$, hence $\alpha = 3.96 \cdot 10^{-7} (s^{-1})$. The resulting trajectories of (22) matched with those presented in van Steekelenburg et al. (2011, p. 23).

REFERENCES

Andersson, J. A. E., Gillis, J., Horn, G., Rawlings, J. B., & Diehl, M. (2019). CasADi: A software framework for nonlinear optimization and optimal control. *Mathematical Programming Computation*, 11(1), 1–36. <https://doi.org/10.1007/s12532-018-0139-4>

de Jong, T. (1990). Natural ventilation of large multi-span greenhouses. Wageningen University & Research. <https://library.wur.nl/WebQuery/wurpubs/fulltext/206452>.

de Zwart, H. F. (1996). *Analyzing Energy-Saving Options in Greenhouse Cultivation Using A Simulation Model*.

Dueck, T. A., Janse, J., Eveleens, B. A., Kempkes, F. L. K., & Marcelis, L. F. M. (2012). Growth of tomatoes under hybrid LED and HPS lighting. *Acta Horticulturae*, 952, 335–342. <https://doi.org/10.17660/ActaHortic.2012.952.42>

Eker, S., Rovenskaya, E., Obersteiner, M., & Langan, S. (2018). Practice and perspectives in the validation of resource management models. *Nature Communications*, 9(1), 5359. <https://doi.org/10.1038/s41467-018-07811-9>

Ferentinos, K. P., & Albright, L. D. (2005). Optimal design of plant lighting system by genetic algorithms. *Engineering Applications of Artificial Intelligence*, 18(4), 473–484. <https://doi.org/10.1016/j.engappai.2004.11.005>

Gómez, C., & Mitchell, C. A. (2014). Supplemental lighting for greenhouse-grown tomatoes: Intracanopy LED Towers vs. Overhead HPS lamps. *Acta Horticulturae*, 1037, 855–862. <https://doi.org/10.17660/ActaHortic.2014.1037.114>

Heuvelink, E. (Ed.). (2018). *Tomatoes* (2nd ed.). CABI. <https://doi.org/10.1079/9781780641935.0000>.

Heuvelink, E., & Challa, H. (1989). Dynamic optimization of artificial lighting in greenhouses. *Acta Horticulturae*, 260, 401–412. <https://doi.org/10.17660/ActaHortic.1989.260.26>

HSL. (2019). HSL, a collection of Fortran codes for large-scale scientific computation. See <http://www.hsl.rl.ac.uk>.

Ji, Y., Ouzounis, T., Courbier, S., Kaiser, E., Nguyen, P. T., Schouten, H. J., Visser, R. G. F., Pierik, R., Marcelis, L. F. M., & Heuvelink, E. (2019). Far-red radiation increases dry mass partitioning to fruits but reduces Botrytis cinerea resistance in tomato. *Environmental and Experimental Botany*, 168, 103889. <https://doi.org/10.1016/j.envexpbot.2019.103889>

Katzin, D., Marcelis, L. F. M., & van Mourik, S. (2021). Energy savings in greenhouses by transition from high-pressure sodium to LED lighting. *Applied Energy*, 281, 116019. <https://doi.org/10.1016/j.apenergy.2020.116019>

Katzin, D., van Mourik, S., Kempkes, F., & van Henten, E. J. (2020). GreenLight – An open source model for greenhouses with supplemental lighting: Evaluation of heat requirements under LED and HPS lamps. *Biosystems Engineering*, 194, 61–81. <https://doi.org/10.1016/j.biosystemseng.2020.03.010>

Kempkes, F. L. K., Janse, J., & Hemming, S. (2014). Greenhouse concept with high insulating double glass with coatings and

new climate control strategies; from design to results from tomato experiments. *Acta Horticultae*, 1037, 83–92. <https://doi.org/10.17660/ActaHortic.2014.1037.6>

Kuijpers, W. J. P., van de Molengraft, M. J. G., van Mourik, S., van 't Ooster, A., Hemming, S., & van Henten, E. J. (2019). Model selection with a common structure: Tomato crop growth models. *Biosystems Engineering*, 187, 247–257. <https://doi.org/10.1016/j.biosystemseng.2019.09.010>

Kusuma, P., Pattison, P. M., & Bugbee, B. (2020). From physics to fixtures to food: Current and potential LED efficacy. *Horticulture Research*, 7(56). <https://doi.org/10.1038/s41438-020-0283-7>

Lee, S. Y., Kwon, J. K., Park, K. S., & Choi, H. G. (2014). The effect of LED light source on the growth and yield of greenhouse grown tomato. *Acta Horticultae*, 1037, 789–794.

Nelson, J. A., & Bugbee, B. (2015). Analysis of environmental effects on leaf temperature under sunlight, high pressure sodium and light emitting diodes. *PLoS One*, 10(10), Article e0138930. <https://doi.org/10.1371/journal.pone.0138930>

Olle, M., & Virsile, A. (2013). The effects of light-emitting diode lighting on greenhouse plant growth and quality. *Agricultural and Food Science*, 22(2), 223–234.

Ramírez-Arias, A., Rodríguez, F., Guzmán, J. L., & Berenguel, M. (2012). Multiobjective hierarchical control architecture for greenhouse crop growth. *Automatica*, 48(3), 490–498. <https://doi.org/10.1016/j.automatica.2012.01.002>

Seginer, I., van Beveren, P. J. M., & van Straten, G. (2018). Day-to-night heat storage in greenhouses: 3 Co-generation of heat and electricity (CHP). *Biosystems Engineering*, 172, 1–18. <https://doi.org/10.1016/j.biosystemseng.2018.05.006>

Stanghellini, C., & de Jong, T. (1995). A model of humidity and its applications in a greenhouse. *Agricultural and Forest Meteorology*, 76(2), 129–148. [https://doi.org/10.1016/0168-1923\(95\)02220-R](https://doi.org/10.1016/0168-1923(95)02220-R)

van Beveren, P. J. M., Bontsema, J., van Straten, G., & van Henten, E. J. (2015). Optimal control of greenhouse climate using minimal energy and grower defined bounds. *Applied Energy*, 159, 509–519. <https://doi.org/10.1016/j.apenergy.2015.09.012>

van Beveren, P. J. M., Bontsema, J., van Straten, G., & van Henten, E. J. (2019). Optimal utilization of a boiler, combined heat and power installation, and heat buffers in horticultural greenhouses. *Computers and Electronics in Agriculture*, 162, 1035–1048. <https://doi.org/10.1016/j.compag.2019.05.040>

van Henten, E. J., & Bontsema, J. (2009). Time-scale decomposition of an optimal control problem in greenhouse climate management. *Control Engineering Practice*, 17(1), 88–96. <https://doi.org/10.1016/j.conengprac.2008.05.008>

van Straten, G., Challa, H., & Buwalda, F. (2000). Towards user accepted optimal control of greenhouse climate. *Computers and Electronics in Agriculture*, 26(3), 221–238. [https://doi.org/10.1016/S0168-1699\(00\)00077-6](https://doi.org/10.1016/S0168-1699(00)00077-6)

van Steekelenburg, A., Hoogervorst, W., & van Antwerpen, A. (2011). Inventarisatie Thermische Wateropslagsystemen. HAS Kennistransfer. <https://library.wur.nl/WebQuery/groenekennis/2070634>. <https://edepot.wur.nl/286897>.

van Ooteghem, R. J. C. (2007). *Optimal control design for a solar greenhouse* (Ph.D Thesis). Wageningen University.

Tap, F. (2000). *Economics-based optimal Control of greenhouse tomato crop production* (Ph.D Thesis, Issue September). Wageningen University.

van der Velden, N., & Smit, P. (2019). *Energiemonitor van de Nederlandse glastuinbouw 2018*. <https://doi.org/10.18174/505786>

Vanhoor, B. H. E. (2011). *A model-based greenhouse design method* (Ph.D Thesis). Wageningen University.

Vanhoor, B. H. E., van Henten, E. J., Stanghellini, C., & de Visser, P. H. B. (2011). A methodology for model-based greenhouse design: Part 3, sensitivity analysis of a combined greenhouse climate-crop yield model. *Biosystems Engineering*, 110(4), 396–412. <https://doi.org/10.1016/j.biosystemseng.2011.08.006>

Vermeulen, P. C. M. (2016). *Kwantitatieve Informatie voor de Glastuinbouw 2016-2017*. Business Unit Glastuinbouw: Wageningen University & Research.

Wächter, A., & Biegler, L. T. (2006). On the implementation of an interior-point filter line-search algorithm for large-scale nonlinear programming. *Mathematical Programming*, 106(1), 25–57. <https://doi.org/10.1007/s10107-004-0559-y>

Xu, D., Du, S., & van Willigenburg, L. G. (2018). Optimal control of Chinese solar greenhouse cultivation. *Biosystems Engineering*, 171, 205–219. <https://doi.org/10.1016/j.biosystemseng.2018.05.002>

Xu, L., Wei, R., & Xu, L. (2019). Optimal greenhouse lighting scheduling using canopy light distribution model: A simulation study on tomatoes. *Lighting Research and Technology*, 52(2), 233–246. <https://doi.org/10.1177/1477153519825995>